SO_2 Gas Abatement Using Ionic Liquids for Marine Applications

by

Pathik Daxeshkumar Patel

A thesis
presented to the University of Waterloo
in fulfillment of the
thesis requirement for the degree of
Master of Applied Science
in
Chemical Engineering

Waterloo, Ontario, Canada, 2018

AUTHOR'S DECLARATION

I hereby declare that I am the sole author of this thesis. This is a true copy of the thesis, including any required final revisions, as accepted by my examiners.

I understand that my thesis may be made electronically available to the public.

Abstract

Sulphur dioxide (SO_2) emission has become one of the major challenging issues for clean marine transportation globally and especially in zero discharge zones Canada-wide with the implementation of the International Maritime Organization (IMO) regulations. Currently, as per the IMO guidelines, zero-discharge scrubber technology is in use for the ships that operate on low cost high sulfur (3.5% w/w) heavy fuels. One of the main concerns with these scrubber technologies is the non-recyclability of the absorbent and high demand for onsite waste storage which takes a toll on process operating cost and cargo space.

Owing to its high capacity, specific selectivity, recyclability, good thermodynamic properties and thermal stability, Ionic Liquids (ILs) can be used as an alternative solvent and need to be tested to get measurable laboratory data. IMO regulations state that SO_2 content release should be within 52 ppm as compared to about 1800 ppm of sulfur oxides in typical exhaust flue gas streams. For this, lab scale experiments were performed with a selected group of ILs to understand the absorption-desorption capacity of one such ionic liquids. One IL, named IL-A, was selected for it better performance and was further studied to better understand the reaction mechanism between the IL and SO_2. Results were quite promising with good amount of SO_2 absorption and partial regenerative desorption of the solvent mixture.

Based on the results, it was evident that the viscosity of the IL-A increased tremendously due to SO_2 dissolution, which necessitated the use of an additive (additive B) as a diluent. The dilution effect on vapor-liquid-equilibrium (VLE) and other physical properties were experimentally analyzed. TGA and FTIR gave some insights to quantify the amount of solvent loss during the recycling process and to learn about thermal properties and the temperature operating range for the absorption-desorption in order to maximize the efficiency.

A mathematical scale-up design model of the absorber to support an actual 20 MW marine vessel combustion engine emitting 61.6 $x10^6$ L/hour of flue gas was developed in MATLAB. Theoretical modelling of the process helped in selecting the ideal packing material and to compare the designed tower with traditional scrubber. For the same scrubber diameter, the designed tower height is about 3 meters higher; however, to reduce the footprint to half, an

increase of 4.6 meters in height is required. Other advantages include lower operating costs, lower solvent requirement and low storage for solvent and waste generation.

Acknowledgements

I would first like to thank my thesis co-supervisors Professor Eric Croiset and Zhongwei Chen of the Department of Chemical Engineering at University of Waterloo. I appreciate their vast knowledge and skills in many areas and continuous encouragement and assistance in writing and editing reports. They consistently allowed this thesis to be my own work, and steered me in the right the direction whenever I seek help.

I would also like to thank the experts at EME-Vancouver who were involved very closely and assisted me with all my questions and queries in my time at National Research Council Canada for this research project: Dr. Eben Dy, Dr. Zhong Xie, Dr. Wei Qu and Mr. Jason Fahlman. Their passionate participation and input have helped me immensely in learning new skills and technology to complete the work for my thesis.

I would also like to acknowledge Dr. Peter Douglas and Dr. Xianshe Feng of the Department of Chemical Engineering at University of Waterloo for taking their precious time out from their busy schedule to serve as external readers of this thesis, and I am gratefully indebted to their very valuable comments on this thesis.

I recognize that this research would not have been possible without the financial assistance of Transport Canada, National Research Council Canada, the University of Waterloo Graduate Studies (Teaching Assistantships), and the Province of Ontario Graduate Research Scholarship fund, and express my gratitude to those agencies.

Finally, I must express my very profound gratitude to my parents and to my sister for providing me with unfailing support to keep me focused and gave continuous encouragement throughout my years of study and through the process of researching and writing this thesis. This accomplishment would not have been possible without them.

Thank you.

Pathik Daxeshkumar Patel

Dedication

Dedicated to my late father Daxeshkumar Patel, my mother Nitaben Daxeshkumar Patel, my sister Bansari Patel and my dear friends.

Table of Contents

List of Figures

List of Tables

Declaration

Upon the National Research Council Canada's request, name of certain chemicals and related data used in the experiments such as the Ionic Liquid and the additive are concealed and are identified as IL-A and additive B experimental data henceforth in this report.

Chapter 1

INTRODUCTION AND MOTIVATION

1.1 Overview

Sulfur oxides (SOx) are one of the major concerns among the air-borne pollutants and greenhouse gases. These pollutant gases have been perpetually blamed for the increasing threat of global warming as well as for natural calamities such as damaging vegetation foliage, acid rains, ocean level rising, flooding, etc. to name a few. Sulfur oxides are not only pessimistic to surrounding environment but also detrimental to human health, flora and fauna. 98 percent of the released SOx gases from the combustion and various other sources are in the form of Sulfur dioxides (SO_2) (Committee on Public Works, 1975). At present, efforts are made to suppress the level of sulfur at the source itself by regulating the sulfur content in the fuel-oil as in pre-combustion and/or by using post combustion technologies such as Flue Gas Desulfurization (FGD).

The problem is greater for the marine transport industries due to more limitation on the reactor design aspect and space availability. The regulations to limit sulfur content in fuel oils have solved the problem partially as it makes the transition for the current consumers far more difficult in terms of retrofitting their current operational methodology and the increased fuel cost. Two types of FGD are used in marine vehicles; Wet and dry FGD ((Air Pollution Control Technology Fact Sheet). Of the two, Wet FGD using lime slurry is more popular within the industry at the moment. However, this causes damaging consequences such as corrosion, scaling and also higher operational cost in terms of consumption and storage of the sorbents. Also, the non-recyclability of the reaction demands for the excess space to accommodate the onsite waste that is generated.

There have been a very few research done (Akyalcin, 2010) (Kohl & Nielsen, 1997) in this direction, particularly to come up with an effective, recyclable solvent to remove SO_2 from the flue gas stream. Ionic liquids especially the Room Temperature Ionic Liquids (RTILs) are one type of the solvents to be looked at (Wen Li, 2017). Due to their excellent physical and thermodynamic properties, low vapor pressure etc. these solvents can be the solution of this very problem. Moreover, Ionic Liquids (ILs) are green causing low to zero damage to environment and are tailored solvents i.e. their properties can be customized by selecting appropriate pair of anion-cation to suit a particular operation.

Recent success of ILs for post combustion CO_2 capture (Matthew S. Shannon, Reactive and Reversible Ionic Liquids for CO2 Capture and Acid Gas Removal, 2012) (Elena Torralba-Calleja, 2013) (Joan F. Brennecke, 2010) reinforced the confidence to conduct trials of using it for SO_2 abatement operation. These task- specific solvents are needed to be screened and tested in laboratory to analyze the chemical and physiological properties, mechanism, process design and optimization to present a real-life process implementation.

1.2 Overall Project objectives

The main objective of this research is to provide an alternate regenerative SO_2 scrubbing technology using Ionic Liquids that can further be able to upscale for real life size process applications. By providing Ionic Liquids as a recyclable solvent option, not only will the operational cost be cut down, problems such as scaling and space constraints will be indirectly solved.

As per the new stringent regulation imposed by International Maritime Organization, the target SO_2 exit concentration should not be more than 52 ppm. In order to achieve this target, the overall project is categorized to achieve 4 main objectives.

- **Screening of the suitable Ionic Liquid**; based on literature review, first principle modelling and SO_2 compatibility/selectivity
- **Testing of physical and chemical properties**; such as viscosity, density, surface tension, TGA, Equilibrium data, FTIR
- **Steady state lab scale operation**; of Absorption-desorption cycling
- **Upscale Design modelling and optimization;** mathematical process modelling in MATLAB to determine the optimum packing material and actual size of the towers.

This thesis will have major emphasis on the property analysis and reactor design aspect to give the best understanding of the aspects of using IL-A for real life implementation.

1.3 Thesis Structure

This thesis includes the systematic work done over the proposed project including Literature review, Experimental design and setup, theoretical mathematical modelling in MATLAB, experimental results and conclusions.

Chapter 2 includes a thorough literature review of the present and updated legislations and current SO_2 abatement technologies being employed in industries. Furthermore, study on as to why the Ionic Liquids should be employed based on its properties and previous research is done systematically to understand its behavior in presence of various gases.

Chapter 3 is devoted to experimental testing for physical and chemical properties of IL. It describes the experimental setup, its procedure and preparation of necessary chemical mixtures along with the purpose of finding such data for process design.

Chapter 4 focuses on the analysis of the data obtained by performing the laboratory experiments and gives more insight on the usefulness of these data, its behavior and quantification and mechanism of reaction of SO_2 in presence of the ionic liquid.

Chapter 5 contains discussion on theoretical mathematical modelling of the absorption tower that is done using MATLAB and discusses about the design aspect of the scale up. It gives the highlight of the selection of the packing materials for the best efficiency and an insight of the space requirement in comparison to scrubbers used in the traditional processes.

Chapter 6 sums up the thesis with conclusion and emphasizes on the shortcomings during the testing and design modelling and propose some future scope to explore in order to quickly escalate the design into real operation.

Chapter 2
LITERATURE REVIEW

2.1 Current Scenario

2.1.1 IMO Regulations

International Maritime Organization (IMO) is a specialized agency of United Nations which is responsible for setting global standards accounting for environmental performance, safety and security of the international shipping industry. Almost all aspects of international shipping which includes ship design, construction, equipment, manning, operation and disposal is covered by IMO to ensure that this vital sector for global marine industry remains safe, environmentally sound, energy efficient and secure.

As per the MARPOL Annex VI (Prevention of Air Pollution from Ships) that was first adopted in 1997, main air pollutants contained in ships exhaust gas, including sulfur oxides (SOx) and nitrous oxides (NOx) are limited and it completely prohibits the deliberate emissions of ozone depleting substances (ODS). Under the revised MARPOL Annex VI, the global sulfur cap will be reduced from current 3.50% to 0.50%, effective from 1 January 2020, subject to a feasibility review to be completed no later than 2018. These caps are even stricter inside the Emissions Control Areas (ECAs) shown in Figure 1; which includes all the Canadian lakes, where the limit of 0.1% is effective from 1 January 2015.

The standard regular fuel used in the ships has about 3.5% sulfur (S) content, which upon complete combustion would produce about 1881 ppm of Sulfur oxides (~ 1800 ppm SO_2) (AP-42 VOL. I: 1.3). In order to meet the mandate, one of the possible options is to switch to very high cost Ultra Low Sulfur containing Fuel Oil (ULSFO) containing less than 0.1% S content or to revamp and

improve the gas scrubbing technology. The ULSFO cost is significant (about $ 300-400 per ton of fuel oil) and may not be acceptable to majority of the industry. So, it is inevitable to improve the scrubbing technology in such a way that scrubbing efficiency offsets the solvent cost.

Figure 1 MARPOL Annex VI Emission Control Areas

2.2 Flue Gas Desulfurization

Flue gas desulfurization is a process to remove sulfur and its oxides from the flue gas mixture before they are sent to the next process or released into the atmosphere. Most of the present scrubbers use an alkali either in the form of slurry or sprayed in form of dry powder. The alkali is used owing to the acidic nature of the sulfur dioxide gas. The reaction between the alkali and the acidic gas yields alkali sulfites. There are basically 2 types of scrubbing technologies available for marine vehicles namely wet scrubbing (A.V. Slack, 1972) and dry scrubbing (Sargent and Lundy LLC, 2002) and the former is further classified into three as open loop, closed loop and hybrid design.

2.2.1 Wet Scrubbing:

Open Loop Scrubbers

These types of scrubbers are relatively simple in design and use sea water to scrub the SO_2 gas. The wash water is then discharged back into the sea without any further treatment; resulting in parasitic load on the ship. The typical chemistry involved is:

$SO_2 + H_2O \rightarrow H_2SO_3$ (sulphurous acid) $\rightarrow H + HSO_3$ (bisulphite)

HSO_3 (bisulphite) $\rightarrow H + SO_3$ (sulphite)

SO_3 (sulphite) + ½ $O_2 \rightarrow SO_4$ (sulphate)

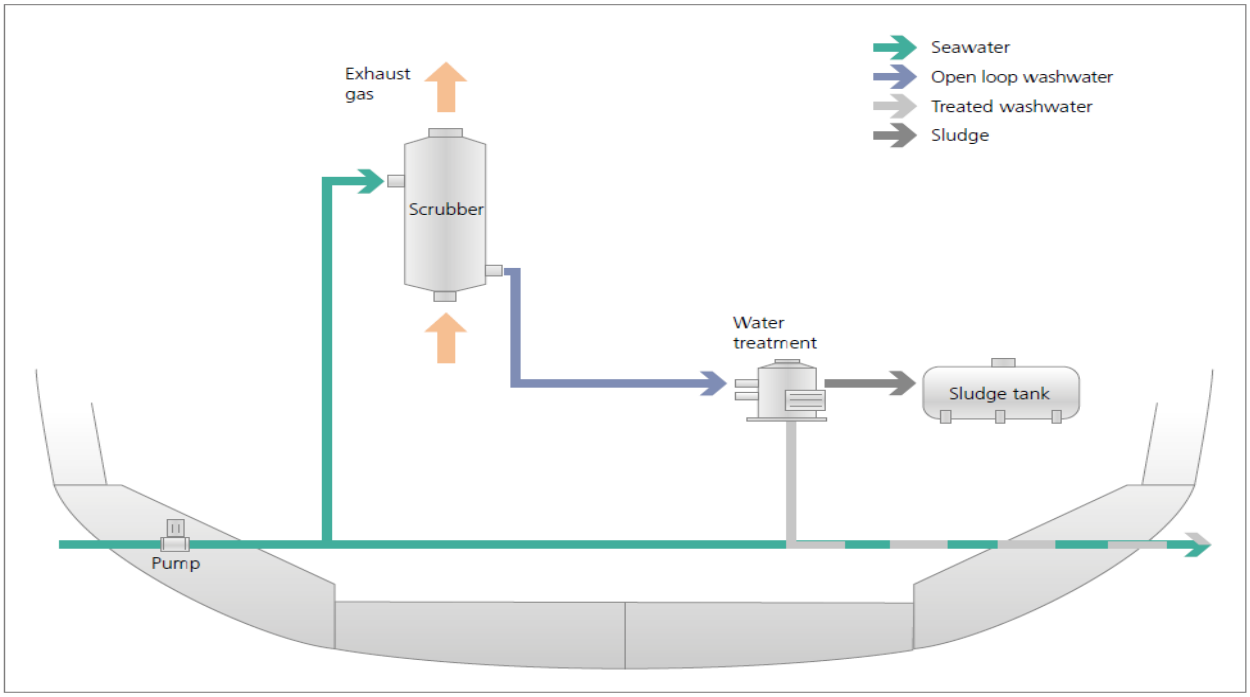

Figure 2 An open loop scrubber arrangement

Closed loop scrubbers:

Closed loop scrubbers are typically used in the ECAs where discharge is not allowed especially in to the ports, harbors and estuaries. Alkalis such as sodium hydroxide, magnesium oxide and sodium bi-carbonate are used for the chemical treatment of the wash water so that the treated water can be recirculated. The reactions go as follows:

SO_2 + 2 NaOH (sodium hydroxide) → Na_2SO_3 (sodium sulfite) + H_2O

$Na_2SO_3 + H_2O + SO_2 \rightarrow 2NaHSO_3$ (sodium bisulfite)

$2NaOH + CO_2 \rightarrow Na2CO_3$ (sodium carbonate) + H_2O

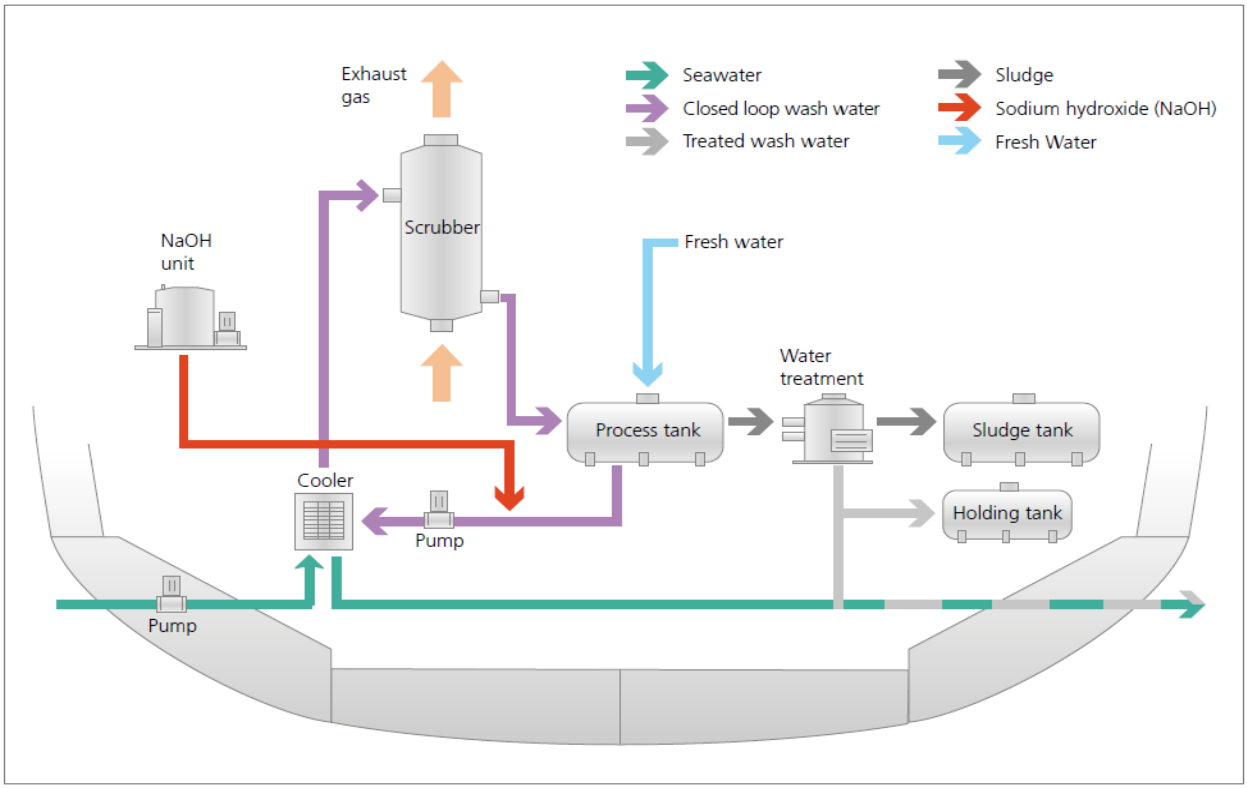

Figure 3 A closed loop scrubber arrangement

Usually, small amount of the alkali carbonates is released to maintain the concentration of sodium sulfate. This can be completely avoided by adding a holding tank to operate in zero discharge regions. Since there is less wash water discharge, the parasitic load is less but the space requirement is more due to the need of buffer tank and holding tank in Zero Discharge Mode.

Hybrid scrubbers

These scrubbers are designed to operate in either open or closed loop depending on the requirement based on the area of operation. This enables the controlled use of the alkali; there by reducing the requirement, storage and associated costs and the use of fresh water. Due to such flexibility, this is the preferred choice among the operators.

2.2.2 Dry Scrubbing:

These scrubbers differ from the wet loop in terms of the state of the sorbent used to scrub the SOx gas. This method is predominant in land FGD but is also used in marine industry using granulated calcium hydroxide instead of conventional powdered form. This granular texture allows to be less bulky than the powder, but the input cannot be varied and are pre-set to operate at maximum continuous rating (MCR).

Dry scrubber residue is calcium sulfite which usually proceeds further to form gypsum and this solid is not dumped into the water like the wet loop scrubbers. This indeed demands for the large storage areas. In terms of footprint, this system takes up greater area and increases the deadweight significantly of the ship. However, the power consumption is quite low in comparison and since there is no residual dumping into waters; it can be used in all the routes (including ECAs.)

2.2.3 Challenges for The Wet and Dry Systems:

Though this method eliminates up to 99% of SOx, it comes with a lot of challenges associated with it. Some of significant ones are mentioned in the following:

Environmental impact of wash water:

The release of the acidic wash water was associated to acidification of seas and ocean. However, this effect is negligible considering the alkalinity of the ocean and sea water which will easily neutralize the former. Having said that, in the ECA regions, this can cause measurable impact on the aquatic life.

Corrosion and scaling:

Since SOx scrubber wash water is highly acidic it requires the use of suitable corrosion resistant piping and for all the surfaces in contact. The sulfites and sulfates cases scaling on the sides of the metal tubing causing back pressures in the operations.

Stability:

The stability of the ships is very important and is challenged here due to requirement of large number of tanks. This results in increased dead weights thus resulting in reduced overall ship efficiency.

2.3 Ionic Liquids in Gas Abatement Processes

Ionic liquids or commonly known as Room Temperature Ionic Liquids (RTILs) are ionic salt that are usually in the liquid states at temperatures 100°C and below. These ILs consists of anions and

cations that are attached with ionic bonds i.e. stronger than Van der Waals forces. Ionic liquids have gained much popularity in recent times due to its unique set of properties and wide range of applications.

Ionic liquids are viscous and have very low vapor pressure in order of 10^{10} Pa at room temperatures and are good conductors of electricity; hence are excellent choice for battery research/operations. Though being in a liquid state at room temperature, they have high thermal stability well over 150ºC – 400ºC depending on the length of the side of cation and choice of anion. Ionic liquids offer a wider choice and are occasionally called designer solvent as they can be designed/custom-made for a specific task to suit its optimum operation. This leverages researchers to expand its application in various dimensions of science.

In recent times, ILs have been studied for CO_2 capture technology with significant interest and research shows that imidazolium based ionic liquids (Joan F. Brennecke, 2010) (Matthew S. Shannon, Properties of Alkylimidazoles as Solvents for CO2 Capture and Comparisons to Imidazolium-Based Ionic Liquids, 2011) show greater CO_2 absorption capacity. It is very well observed that anions primarily dictate the absorption capacity and stronger Lewis bases such as IL-As (L), acetates (Ac), and halogens absorb more acidic gases in comparison to weak Lewis bases (TFSI, BF_4 and PF_6). For task-specific ILs, the cation can also contribute significantly to SO_2 absorption.

ILs have also dictated great reversibility by applying pressure or temperature swing while exploiting its application for CO_2 capture. Formulating task specific ILs will not only enable to explore similar applications for other gases especially the SO_X and NOx individually but can even enable us to use it for a combination of gases at the same time. It has been debated time and again

about the biodegradability of certain types of ILs, however this issue can be subdued for a long period of time as these are mostly reversible in nature and generate a very little to no waste in the process.

2.4 Current Progress

Seeing the immense potential in this area, the Energy, Mining and Environment portfolio at National Research Council, Canada and University of Waterloo, Canada, with the funding support from Transport Canada undertook the challenge to determine ILs as suitable candidates and present a good process design to translate the theoretical evidence into reality. Since the project inception, the scrutiny of various Ionic Liquids was carried out based on rigorous First principle modeling, DFT and Monte Carlo simulation methods to narrow down a few candidates for laboratory testing.

Initially, Imidazolium based Ionic Liquids showed the highest likeness to be chosen as a cation and previous work by Modal et. al. (Anirban Mondal, 2016) and Ghobadi et. al. (Ahmadreza. F. Ghobadi, 2011) supported this. At first, testing was initiated with other IL. It was tested for recyclability, capacity, solubility and effects of presence of water (National Research Council Canada, 2015). Results showed good absorption-desorption capacity but it was severely affected by the presence of water content along with very high amount of foaming was a major issue with this IL. Consequently, custom made, IL-A was tried and it showed much higher capacity and good recyclability.

IL-A anion being a strong Lewis base which has enabled higher primary SO_2 affinity in association with secondary support from the imidazolium cation. To investigate its usability and form a preliminary process design, a rigorous laboratory testing to analyze the physical and chemical properties and reversibility of this ionic liquid was initiated. The motive of this thesis is in

alignment to the vision of providing and proving that ILs can be an efficient alternative solvent for desulfurization operation.

2.5 Knowledge Gap

As mentioned in the above sections, there have been attempts made to diminish the SO_2 release into the atmosphere. But the current technology is too fragile to keep up with the updated stringent regulations. The technology is around but it is needed to be upgraded to suit the current perspective and to make sure that this survives at least for a foreseeable future and is well within the financial and atmospheric constraints.

Ionic liquids can be the candidate theoretically for the FGD but there is not much research available to support the fact. They have advantages over the conventional SO_2 solvents: firstly, they can be designed task-specifically which will give the freedom to explore multiple options and secondly, they are reported as to be green solvents which ensure that if will not have any harsh impact on the mother nature. Also, looking in the Ionic Liquid characterization and properties, it might help explore further applications into similar other gas abatement technologies.

Ionic liquids use for similar CO_2 abatement have been well studied and one simulation research study by mark et. al. (Shiflett, Drew, Cantini, & Yokozeki, 2010) shows that it can significantly reduce the size of the reactors by 12% footprint as well as the operational and capital cost by 11% than traditional MEA process. It would be great to be able to translate these advantages for SO_2 abatement but it would require careful examination and screening of the Ionic liquids out of all the possible permutation and combinations of anions-cation pair possible (10^{18} possibilities). Experimental data will also assist in understanding the selectivity of the SO_2 gas in presence of a mixture of gases at lower partial pressure.

By abridging this, new windows for optimization and design modifications will be enabled for more transparent understanding.

2.6 Thesis Objectives

Ionic Liquids is a relatively new area especially for the flue gas desulfurization processes. Not much research has been done in this direction except a few that looks into the properties of ionic liquids individually and with respect to post combustion carbon capture technology. Having said that, taking inspiration from this limited literature, we have decided to move a step forward to explore its application to FGD process.

The main objective of the thesis is to propose and demonstrate a promising process technology of the usefulness of the IL in selective gas separation. The goal is to test the IL for various property testing and use the data to simulate the process taking a real marine diesel engine to prove the capacity. This research will help future researchers as a starting point for further refining the process and develop more-efficient other task specific ILs in future.

The work looks at the equilibrium, electrochemical and cyclic testing of the proposed ILs along with physical and chemical property testing and characterization. Furthermore, mathematical modelling will help selection of suitable packing materials and estimating overall dimension of the absorption tower.

Chapter 3
MATERIALS, PROPERTIES & CHARACTERISATION

3.1 Materials

3.1.1 Ionic Liquid A (IL-A)

From prior screening by NRC of a few ionic liquids based on first principle modelling and testing, IL-A was chosen as one of the most suitable candidates for basic testing and for developing the design of an IL-A based SOx scrubber. IL-A can be manufactured in a one-stage synthesis without much of the by-product by combining IL-A anions from inexpensive and simple reactants. However, the purification process; i.e. removal of moisture from ionic liquid, is quite tedious.

IL-A used was custom-made with a certified purity greater than 98% by IoLiTec Ionic Liquids Technologies GmbH. This product is lightly yellowish brown in appearance and this coloration is usually indicative of the presence of impurities. In most cases, these trace impurities are extremely difficult to remove but are so minute in quantities that they should not interfere in a larger capacity with IL-A's functionality. However, before testing, all samples of ILs were either purged in nitrogen stream or heated under vacuum at an elevated temperature over a course of 24- 48 hours until the sample weight remains constant to remove any trace volatile impurities. This pre-treatment is also essential owing to the hydrophilic nature of this IL when exposed to humid environment. The water content was analyzed over time using Karl-Fischer titration and was always less than 0.6% w/w.

IL-As, in general, are nontoxic pharmaceuticals and are categorized as Generally regarded as safe (GRAS) materials in FDA database. Longer alkyl chain IL-A cations are, in general, slightly toxic and are not easily biodegradable. However, smaller alkyl chains have minimal toxicity and their

decomposition is also faster by ozonation, hence they can be technically categorized as green solvents.

3.1.2 Additive B (additive-B)

Over the course of the experiments, it was soon realized that the viscosity of the IL upon absorption of the SOx gases increases tremendously. This necessitated using a suitable additive such as additive-B that reduces the viscosity without much interference with the IL. Additive-B used was a pure product (purity greater than 99%) purchased through Aldrich Chemistry. The water content, as determined using Karl Fischer, shows that it is below 0.1%. Since additive-B was of high grade quality, there was no additional purification techniques/procedures applied and was used as is.

The selection of additive-B was supported by previous researches that demonstrated its use for various processes involving SO_2 gas separation (Zhang, et al., 2013). Further details are discussed in section 4.1.1. In conjunction to this, its stability at higher temperature operations and high boiling point were additional beneficial attributes leading to its selection. Solubility tests proved that it mixes well with IL-A and is totally miscible. It was imperative that the additive does not affect the gas absorption capacity and the experimental results helped to support the fact in favor of additive-B.

3.1.3 Sulfur Dioxide (SO_2)

A blend of sulfur dioxide (SO_2) and nitrogen (N_2) gas was obtained from Praxair, Inc. for the operation. In order to match the real operation concentration, an A3 sized gas cylinder was custom-blended to 3.5% SO_2 gas (35,000 ppm) with the balance being pure nitrogen. Experimental concentration for SO_2 had to be 1800 ppm, for which the gas stream was further mixed with a

stream of pure nitrogen gas and the flowrates were accurately adjusted to get the required concentration with an accuracy of ± 20 ppm. The output concentration was confirmed by analyzing it with a digital gas analyzer.

Sulfur dioxide gas being poisonous in nature, was operated with utmost care and the gas cylinder was placed inside a fume hood with multiple sensors and a relay to immediately shut off the gas supply in case of emergency. IL-A was tested previously (National Research Council Canada, 2015) regarding its selectivity toward other gases such as CO_2 and N_2 and it was confirmed that absorption ratio of SO_2 was at least 2 orders of magnitude higher than CO_2 and N_2 at such low concentrations. This selectivity was observed and confirmed with other similar imidazolium based ILs.

3.1.4 Nitrogen (N_2)

Pure nitrogen gas (99.99 % purity) was obtained from Praxair, Inc. and was used as is. It was used in all aspects of the process such as in pre-treatment of IL-A for removing volatile impurities by passing a stream of N_2 gas through IL-A at higher temperature. In the absorption process, it was used to lower the concentration of SO_2 from 35,000 ppm to 1800 ppm. In the desorption process, it was used by passing the pure stream of N_2 at desorption temperatures.

3.2 Unit operations

3.2.1 Absorption

Absorption is a unit operation usually employed in gas-liquid separation processes to preferentially remove a specific gas from its mixtures by using suitable liquid solvent. There are two kinds of absorptions; physical or chemical depending on the nature of reaction. Physical absorption is when

there is no significant chemical reaction between the solute and the solvent and that are easy to separate. Chemical absorption happens when there is appreciable amount of reaction going on in between the species which may form intermediate compounds in the process.

The absorption in the wet and dry FGD is an example of chemical absorption and so they are highly irreversible in nature. This requires the need for the perennial need for the new absorbent, which tends to greatly increase the operational as well as disposal cost of the process. Ionic Liquids, on the other hand offers the advantage of being reversible in nature. This partially solves the above two problems.

The absorption between the Ionic liquids tested and SO_2 gas is slightly complex and is proposed to be a combination of physical and chemical absorption. During experiments, it was observed that not all the absorbed SO_2 is recoverable which suggests that a part of the SO_2 bonds strongly enough by chemical absorption that it cannot be separated feasibly.

3.2.2 Desorption

Desorption is a unit operation employed to recover and recycle back the solvent used in absorption. It works on the same principle as before but the mass transfer in this case is from liquid phase to gas phase. Usually, desorption is undertaken by either temperature or the pressure swing; i.e. either by elevating the temperature or by decreasing the pressure from that used in the absorption process.

The process of absorption-desorption for very dilute solution follows the henry's law of partial pressure. Therefore, at very low partial pressure, it is safe to assume that solubility of the gas is linearly proportional to the partial pressure of the gas. For our system, the absorption was

conducted at lower temperature range (20 to 35°C) and 1 atm. pressure while desorption was carried out at elevated temperatures of 65 to 75°C and/or under vacuum.

3.3 Gas-Liquid Equilibrium Experiments

Finding reliable gas-liquid and vapor-liquid equilibrium data may be the most time-consuming task associated with the design of absorbers and other gas-liquid contactors, and yet it may be the most important task at hand. For the design of the absorption-desorption column, it was necessary to obtain equilibrium data for the process. In order to achieve this, the following experiments were successfully completed.

To carry out both experiments, a specially designed glass tube was fabricated with the help of CanSci Glass Products Limited. The design is shown in Figure 4. The gas mixture enters from the left side and will pass through the diffuser to get in contact with the solvent and then goes out from the right-hand side of the tube through the scrubber before being released into the atmosphere. The diffuser helps the gas to spread evenly and form smaller size bubbles which would allow more contact surface area and retention time for the SO_2- IL. The flowrate of the gases was precisely adjusted by using low flowrate Alicat flowmeters (1-200 sccm range) with greater accuracy. The glass tube was temperature controlled in the water bath with accuracy of ± 0.1°C. All glass wares were thoroughly cleaned with DI water and completely dried in oven before use. The scrubber fluid was 4 molar KOH solution to ensure least amount of SO_2 is released directly during the operation.

The following operating procedure was used during all the equilibrium experiments.

Measure a fixed weight of IL-A in the glass tube.

Pre-treat by passing a stream of pure N_2 gas at 55 – 60ºC to get rid of volatile materials and monitor the weight until it gets constant.

Add 15% (w/w) of the diluent additive-B to the IL and shake well.

Start the stream of SO_2 gas stream at 1800 ppm and adjust the temperature as desired.

Monitor the sample weight periodically until the weight remains constant.

For desorption, shutdown the SO_2 gas stream and adjust the temperature as desired.

Monitor the reduction in weight of sample until it becomes constant.

This procedure was repeated for absorption at temperatures of 25, 35 and 65 °C and desorption temperatures of 25, 35, 45°C to get the data for equilibrium curve calculation.

For physical property experiments, the absorption was done at 35°C and desorption of the similar sample at 85°C.

Fig. Figure 5 Schematics of Abs-Des experimental setup & Figure 6 Operational setup for Abs-Des experiments shows the schematics and actual testing of the equilibrium experiments.

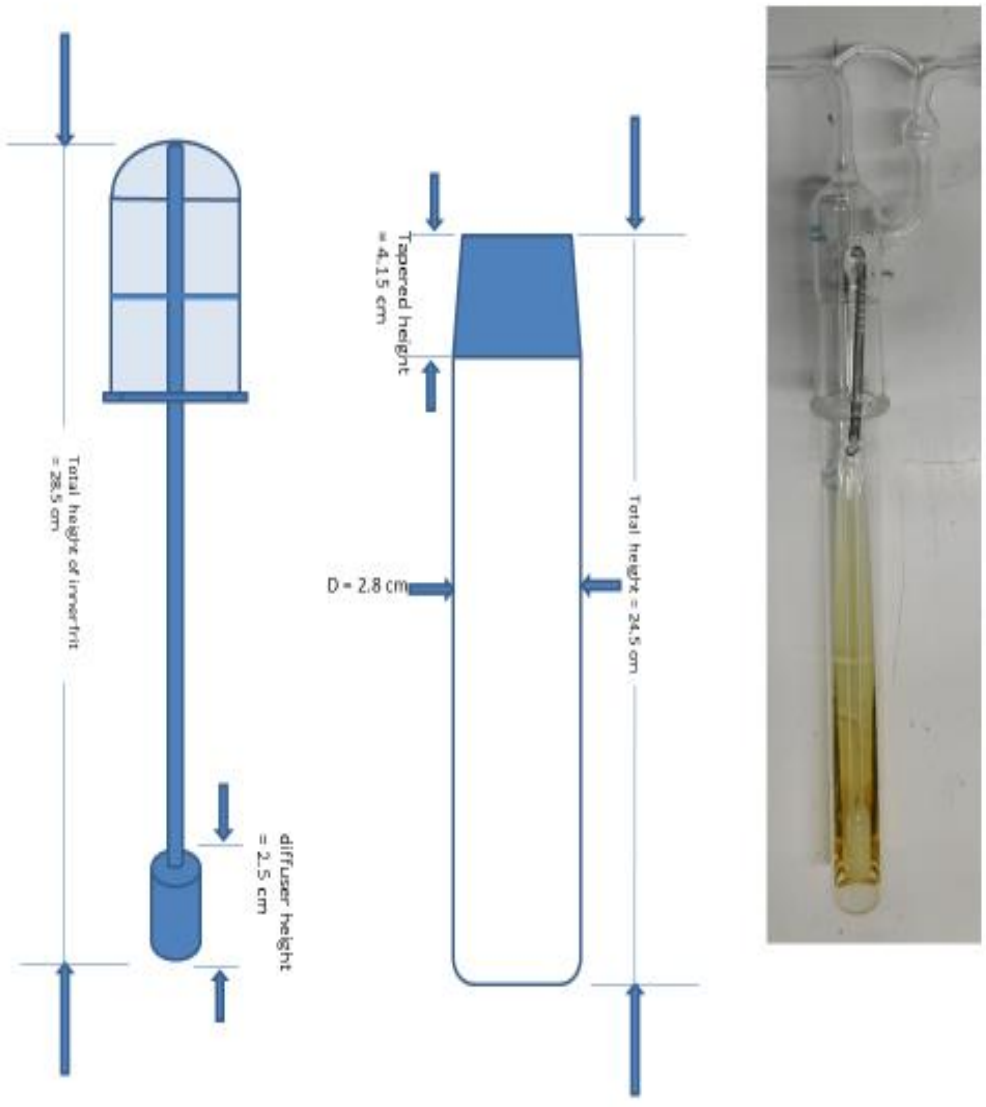

Figure 4 Special designed glass tube for SO_2-IL-A abs-des experiments.

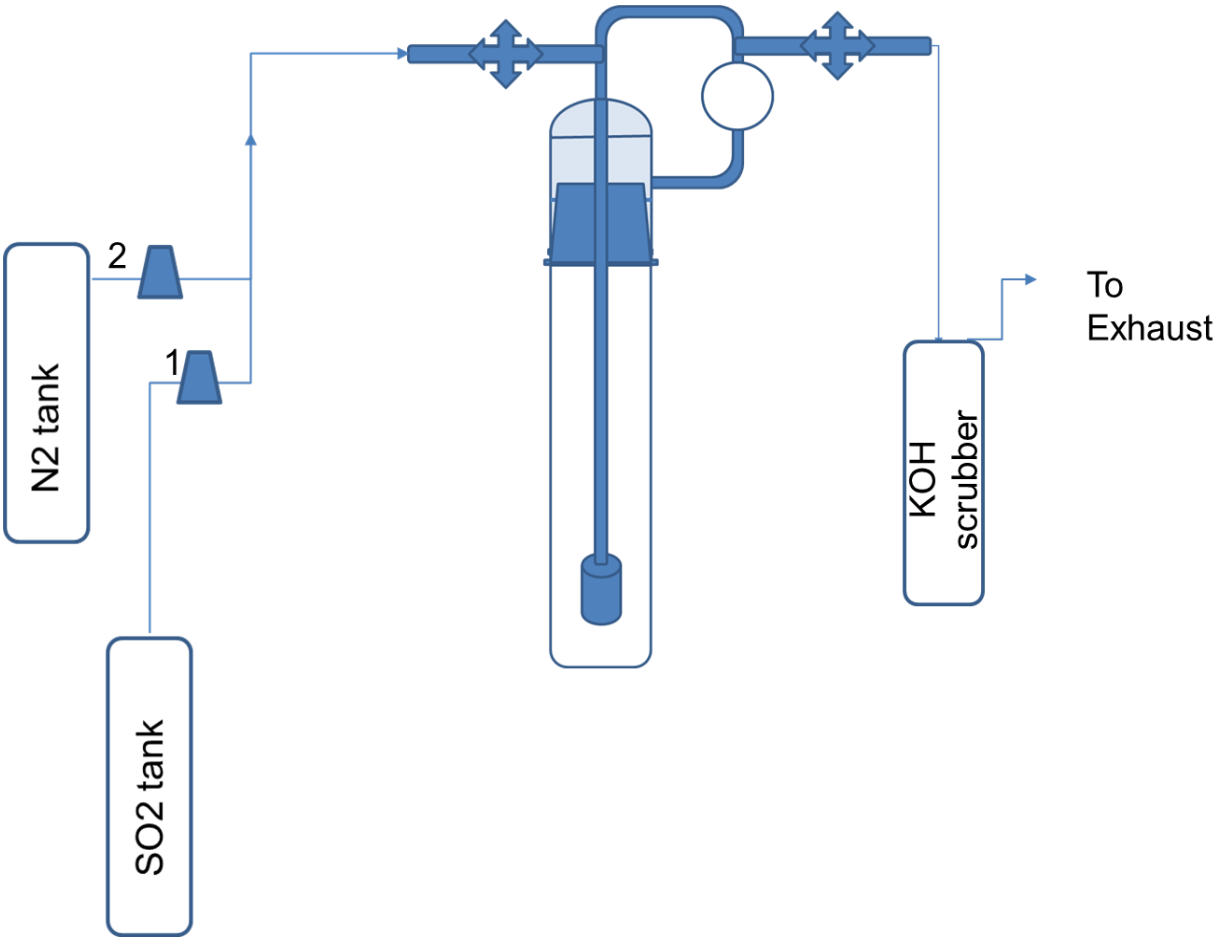

Figure 5 Schematics of Abs-Des experimental setup

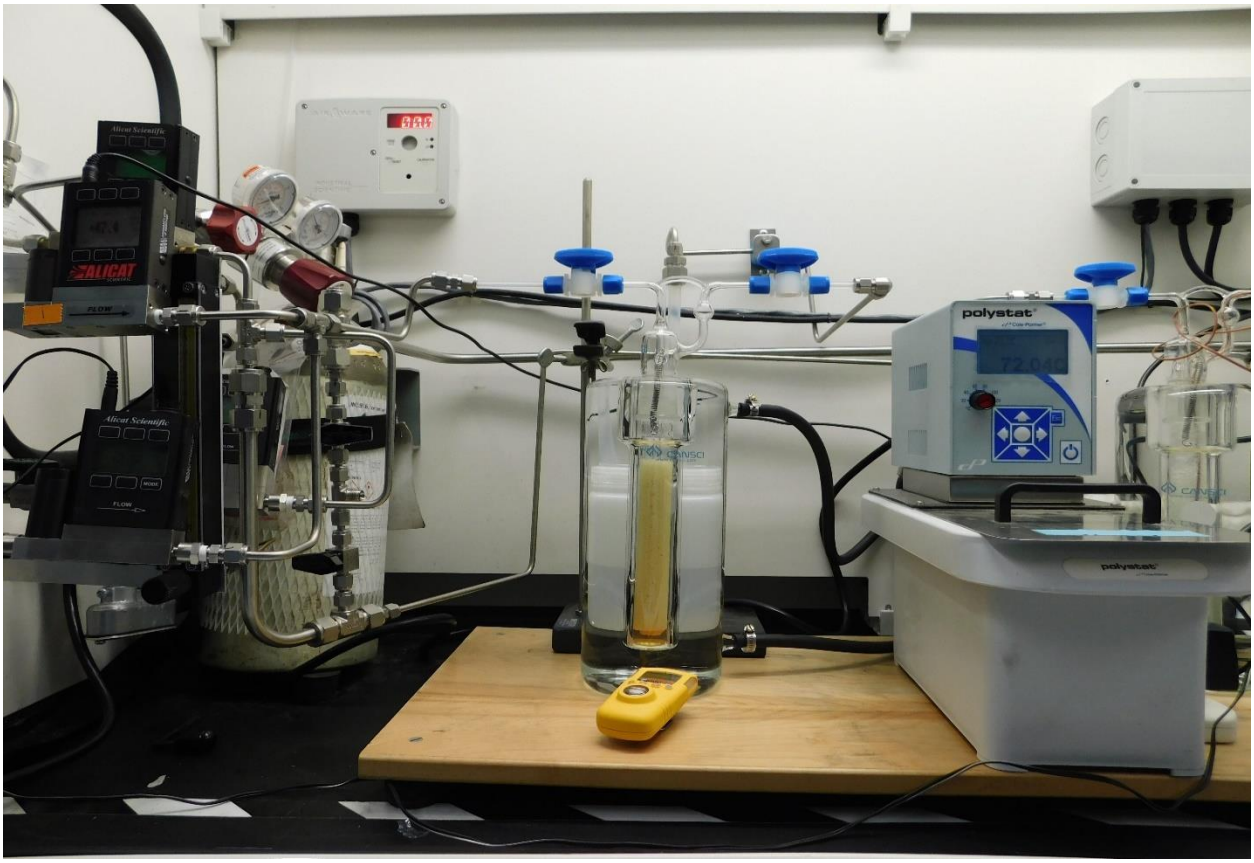

Figure 6 Operational setup for Abs-Des experiments.

3.4 Recyclability Experiments

The purpose of choosing a reversible solvent is to recycle it, so as to lower the operational cost and waste generation. IL-A was tested for recyclability using a smaller sample of about 2 g that was prepared with about 15% w/w of additive-B. The Figure 7 shows the actual recyclability test setup. This IL-A was pretreated to ensure removal of most of the volatile materials through nitrogen purging until the weight remained constant. Three cycles of alternate absorption/desorption were carried out and this sample was analyzed using FTIR, TGA and Karl Fischer titration. The procedures for these experiments are discussed in the following sections of this chapter. To imitate the real process, the absorption temperature was set at 25^{o}C and the

desorption was carried out at 65 and 45°C. The operating procedure is the same as that of the equilibrium experiments. It was suspected that a considerable amount of additive-B is lost at higher temperature and to answer this suspicion, the desorption was carried at different temperatures. This test also aimed at studying the recoverability of IL-A during desorption and the decrease in absorption capacity through different cycles. These analyses are explained in detail in Chapter 4.

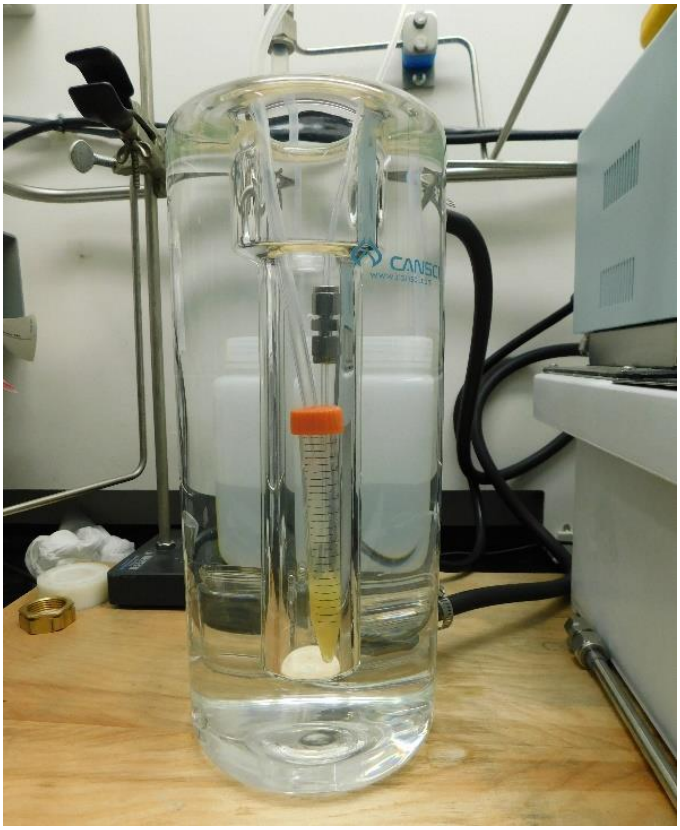

Figure 7 Operational small sample setup for recyclability experiments

3.5 Physical Properties Experiments

The determination of physical properties such as viscosity, density and surface tension is essential. In the process, the change in behavior before and after the gas absorption or desorption should be understood. It is also necessary to know its dependency on the process variables and experimental

conditions, such as temperature and concentration. These data are key for designing such absorption process.

The procedure and the experimental conditions for physical property determination are described next.

3.5.1 Viscosity Measurement:

The viscosities of clean and SO_2-saturated IL-A were obtained with a BROOKFIELD viscometer following standard procedures. The clean IL-A sample was taken directly from the bottle. The SO_2-saturated IL-A samples were obtained from the equilibrium experiments following the procedure mentioned before. The viscosity was measured at various temperatures in the range of 22 to 85°C at atmospheric pressure. The following standard operating procedure (Brookfield Digital Viscometer Model DV-E Operating Instructions) was followed rigorously for each temperature readings.

The water jacket was connected to the water bath and the water was stabilized at the proper temperature:

1) Add the proper amount (0.5 ml) of test sample into the sample chamber.

2) Place the sample chamber into the water jacket.

3) Put the spindle into the test fluid and attach the extension link, coupling nut and free hanging spindle to the DV-E.

4) Allow a few minutes for the sample, sample chamber and spindle to reach test temperature.

5) Measure the viscosity and record the viscometer reading.

The results of the viscosity measurements are summarized and discussed in section 4.1.

3.5.2 Surface Tension Measurement:

Surface tensions were determined with a KSV SIGMA 701 FORCE Tensiometer following a platinum Wilhelmy plate procedure (Standard Operating Procedure for KSV SIGMA 701 FORCE) at various temperatures ranging from 25°C to 85°C at atmospheric pressure. The concept behind this method is simple; the sample surface is lifted until it contacts the lower edge of the plate. The wetting or capillary force pulls liquid up on the surface of the plate until equilibrium is reached. This weight increases to some maximum value which equals the surface tension times the length of the contact line between the plate and the liquid. In order to ensure the complete wetting, the plate is made of roughened platinum. The maximum force needed to pull the ring from the liquid is proportional to the surface tension of the liquid. The greater the force needed the greater is the surface tension.

IL-A with and without 15% additive-B was saturated at 35°C and were desorbed at 85°C. Surface tension of pure additive-B was also determined. The results are summarized in section 4.2.

3.5.3 Density Measurement:

Densities were determined using a KSV SIGMA 701 FORCE Tensiometer following the standard operating procedures. A glass density probe with a standardized known volume is hung from the balance hook and is immersed completely into the sample to be measured. The force needed to hold the probe at a constant depth (20 mm in this case) in the sample is then recorded. The software, using the principle of Archimedes automatically calculates the density of the sample using a number of iterations specified (10 in this case) in the system.

IL-A with and without 15% additive-B was saturated at 35°C and were desorbed at 85°C. The densities of fresh IL-A and additive-B obtained from the bottle were also determined. All experiments were done in a closed environment at atmospheric pressure and temperature controlled using water bath. The results are discussed in section 4.3.

3.6 Cyclic Voltammetry Experiments

Cyclic Voltammetry was performed to determine the diffusion coefficients for this IL-A-SO_2 system using Solartron potentiostat 1287A. The software used for this was CorrWare and CView (Scribner Associates Inc.) and the data was analyzed using Origin 7.1. (OriginLab Corp.) A small sample (8-10 grams) of clean and SO_2 absorbed IL-A was analyzed at different scan rates within a fixed potential window to understand the behavior and the diffusion of the SO_2 at the electrode surface. A 3 electrodes system with platinum microelectrode (100 μm diameter) as a working electrode, Ag/Ag+ as reference electrode and platinum wire (1 mm diameter) was used as control electrodes.

The effective surface area of the working electrode is not always the same as that of area of disk electrode (S.Trasatti & O.A.Petrii, 1992). The true surface area of a working electrode was calibrated by preparing a 0.002 M ferrocene solution in acetonitrile with 0.1 M EMI-TF as a supporting electrolyte. Supporting electrolytes are used to maintain constant ionic strength and are not electroactive in the potentials that are used. (Wang, 2006).

The working electrodes were polished using 3 and 1 μm fine diamond polish, cleaned with methanol, and air dried before putting to use. The reference electrode was carefully stored in the

AgCl solution and internal solution was replaced after testing every three days. The results of CV are discussed in section 4.4.

3.7 Moisture Content Using Karl Fischer Titration

The exhaust flue gases from the engine contains a significant amount of moisture with it. Though, most of the it is lost during the nitrogen oxides removal step using selective catalytic reduction which is generally done at elevated temperatures as a first step in gas removal processes. However, it is still necessary to understand the effect of the presence of moisture on the ionic liquid and to know about whether it is hygroscopic in nature.

The moisture content was measured using Karl Fischer titration (coulometric titration principle) and was done on KF Ti-Touch (Metrohm). The moisture content was monitored before and after the absorption and cycling, as well as for fresh IL-A and additive-B retrieved directly from the bottle. Small samples in milligrams were used for equipment calibration and a larger sample (~ 2 grams) of the mixture sample for water content evaluation. Hydranal Composite 5 was used as the titrant and Hydranal dry methanol was used as solvent. Hydranal standard sodium titrate was used for standardization. Reagents were purchased from Sigma Aldrich and used directly without further preparation. All experiments were carried out in atmospheric pressure and temperature by calibrating the equipment periodically. The results were reproducible and are discussed in the section 4.5.

3.8 Thermogravimetric Analysis (TGA) Experiments

For solvent selection, two important factors to consider are 1) thermal stability, and 2) low vapor pressure solvent to avoid its recovery as an additional step in process design. These properties

were put to test on SETARAM SETSYS EVOLUTION 1750 equipment. To confirm the vapor pressure in terms of amount of solvent lost, isothermal TGA experiments were carried out over the entire range of working temperature. Those experiments were carried out to determine the best operating temperature range, where minimum amount of solvent is lost.

The TGA also gave a sense of thermal stability by obtaining the inflection point using first derivative of the TGA curve. The degradation temperature of IL-A and boiling temperature of additive B were determined as required by ramping up the temperature to 500°C. Analysis of the of the sample after a few cycles gave insights about the changes in the mechanism and capacity of IL for the reaction. In all experiments, a small amount of the sample (about 40 mg) was put in an alumina crucible under inert argon gas environment in order to avoid moisture and other gases interferences. The results are discussed at length in the section 4.6.

3.9 Fourier-Transform Infrared Spectroscopy (FTIR) Experiments

FTIR experiments were conducted independently for fresh, saturated and cycling samples of IL-A-additive-B-SO_2 mixtures. The primary motive of these were to get a better insight of the reaction mechanism and to confirm the presence of and changes in the various components upon absorption and desorption. It was carried out with Nicolet 8700 equipment using Attenuated Total Reflectance (ATR) sampling technique. The required parameters were set using OMNIC software to get precise reproducible signals (4 cm^{-1} resolution).

The samples were analyzed as is and a typical spectrum is shown in Figure 15 and 16. The equipment was calibrated using standard polystyrene film for best accuracy. The surface was

cleaned using DI water and dried prior and in between different samples while analyzing. Fresh samples were prepared and were subjected to FTIR to minimize the atmospheric interference.

With FTIR, it was intended to observe the SO_2 signals before and after the absorption-desorption. Also, predictions regarding the additive-B loss were made by studying the peak height of additive-B spectra. A comparative analysis of the fresh IL-A-additive-B to that of after absorption and 3 cycles also gave some insights. The results are discussed at length in section 4.7.

Chapter 4
EXPERIMENTAL DATA AND ANALYSIS

4.1 Viscosity

The viscosities of fresh and SO_2-saturated IL-A were obtained with a Brookfield viscometer following standard procedure as mentioned in section 3.5.1. The viscosity of fresh IL-A at 35°C is much higher (283.2 cP) than that of water (~1 cP) and it increases even more with the absorption of SO_2 (1253 cP). Even after desorption at 85°C, the viscosity of the desorbed sample remains quite high. This is because SO_2 can only be partially removed. This phenomenon has been observed for other ionic liquids that interact with SO_2 through chemisorption (Zhang, et al., 2013) (Zeng, et al., 2015). On the other hand, the viscosity has been observed to drop when SO_2 is physisorbed (Zeng, et al., 2015). Physisorption, however, is not applicable to flue gas desulfurization as the concentration of SO_2 is very low; like in this case where it is 0.18% (1800 ppm).

Viscosity is an important parameter for reactor design and higher viscosity results in more issues. High viscosity can cause potential backpressure and flooding problems in a packed absorption tower, especially as the flow rate of the IL-A and/or gas mixture is increased. It can also limit the diffusion of SO_2 in the liquid phase due to greater film resistance limiting mass transport. Hence, it is of primary importance to reduce the viscosity, which was achieved using two methods theoretically:

- By elevating the desorption temperature to remove further SO_2;
- By using a suitable additive to improve viscosity.

It was observed during equilibrium experiments that desorption at 85°C starts to darken the IL-A and it was suspected to have initiated the formation of some complex mixture. Though it was not confirmed whether it was due to degradation or formation of something else, it was much easier to consider the second option by carrying out a literature survey to find a suitable additive.

4.1.1 Additives to Improve Viscosity:

In pursuing this option, it was clear that the additive should be compatible with IL-A in a way that it must not affect the absorption/desorption performance capacity. Literature shows that a class of compounds called glycol methyl ethers (glymes) can be used for SO_2 absorption (Sun, Niu, Sun, Xuc, & Wei, 2015) (Schmidt & Mather, 2001) (Xu, Xiao, Zhang, & Wei, 2016). A study by S.Sun et.al. (Sun, Niu, Xu, Suna, & Wei, 2015) has shown that salts like $LiNTf_2$ have been highly efficient for SO_2 absorption. Glymes, being highly polar solvents, allows a good amount to be dissolved in IL-A. Glymes by themselves do not absorb as much SO_2 as ionic liquids or amine solvents. Among all the glymes, additive-B was chosen owing to its low viscosity and low vapor pressure and being readily and cheaply available.

The maximum solubility of additive-B in IL-A was experimentally determined to be 20% by weight. Subsequently, 15% wt. mixtures of additive-B with fresh IL-A and IL-A after desorption at 85°C were prepared. Viscosities were determined at various temperatures ranging from 25 to 85°C. The effect of % additive-B on IL-A viscosity is shown in Figure 8. One can see from this figure that the profiles of viscosity, as a function of %additive-B is well represented by fits an exponential curve.

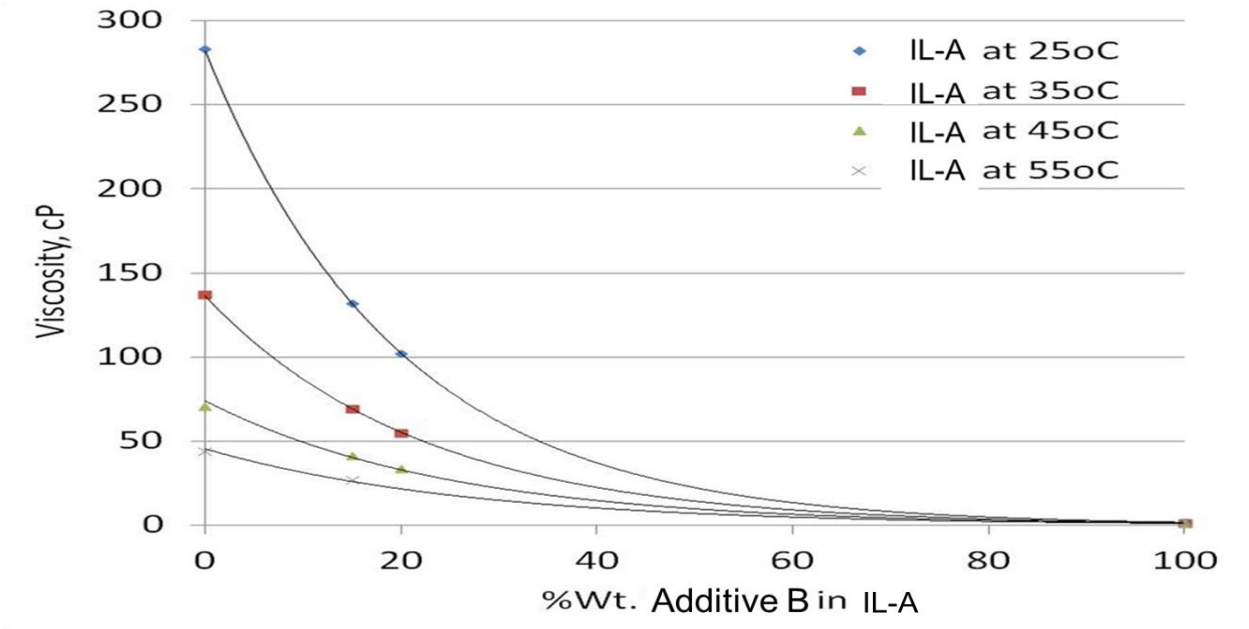

Figure 8 Effect of additive-B addition on IL-A viscosity at various temperatures.

The effect of temperature on viscosity also follows an exponential curve as shown in Figure 9. The effects of temperature and solvent (additive-B) dilution on IL-A and IL-A-SO_2 systems viscosities are typical of ILs and solvent addition. The viscosity drop was more significant for SO_2-containing IL-A. This is expected given that its viscosity difference with additive-B is more significant. Based on the results in Table 1, the improvement by adding 15% of additive-B is roughly equivalent to increasing the temperature by 30°C.

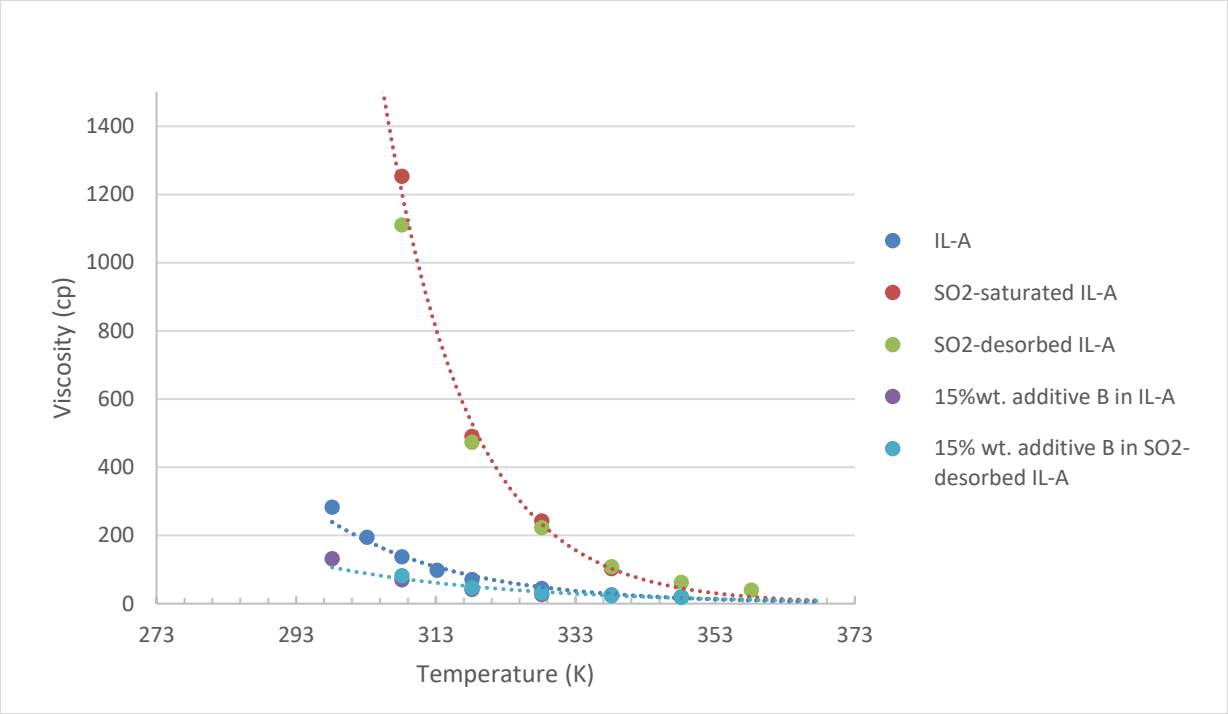

Figure 9 Effect of temperature on the viscosities of various IL-A systems

Table 1 Viscosities (cP) at various temperatures of various solvent-additive ratios after abs-des process.

T, ºC	IL-A	SO_2-saturated IL-A	SO_2-desorbed IL-A	15%wt. additive-B in IL-A	20% wt. additive-B in IL-A	15% wt. additive-B in SO_2- desorbed IL-A	additive-B
25	283.2			132	102		
30	194.2						1.8
35	137.3	1253	1111	69.4	55	81.8	
40	98						1.5
45	71	490	473	41.7	33.7	46.5	
50							1.3

55	44.3	242	222.7	26.9	31.6	
60						1.1
65	25.9	103	108.5		22.9	
70						0.9
75	20.3		62.4		18	
85			39.9			

4.2 Surface Tension

Another important parameter to consider in the mathematical design of towers is the surface tension of the solvent. Lower surface tension aids in the overall mass transfer in a packed tower. However, it is of absolute necessity that the surface tension does not get too low; otherwise, it can induce foaming in the tower. Foaming is detrimental as it leads to higher tower pressure drop which in turn will result in flooding of the tower.

The surface tension measurements are performed as described in section 3.5.2. As a general trend in temperature-surface tension relationship, surface tension decreases with increase in temperature and it is very well confirmed with this system as well. The surface tension tests were performed using Sigma 701 force tensiometer and the results of surface tension at various concentrations ratios of IL-A to diluent additive-B and temperatures are summarized in Table 2.

These experimental results also validate the purpose of the additive; it is clear from Table 2that addition of the additive-B to SO_2 saturated and desorbed samples significantly decreases its surface tension. As seen in Figure 10, increasing temperature also decreases surface tension following a linear trend although the decrease is not as significant as for additive-B addition.

One possible set back of lower surface tension, however, is the increased tendency for foaming. This could be tackled by managing the amount of additive-B added to IL-A to ensure minimum foaming. Addition of 15 % additive-B seemed to have no major implications of foaming during the laboratory equilibrium and reversible testing. Also, instead of N_2 purging for real systems, other desorption techniques such as pressure swing operations like vacuum stripping can be used instead of temperature swing operation to avoid foaming in the towers.

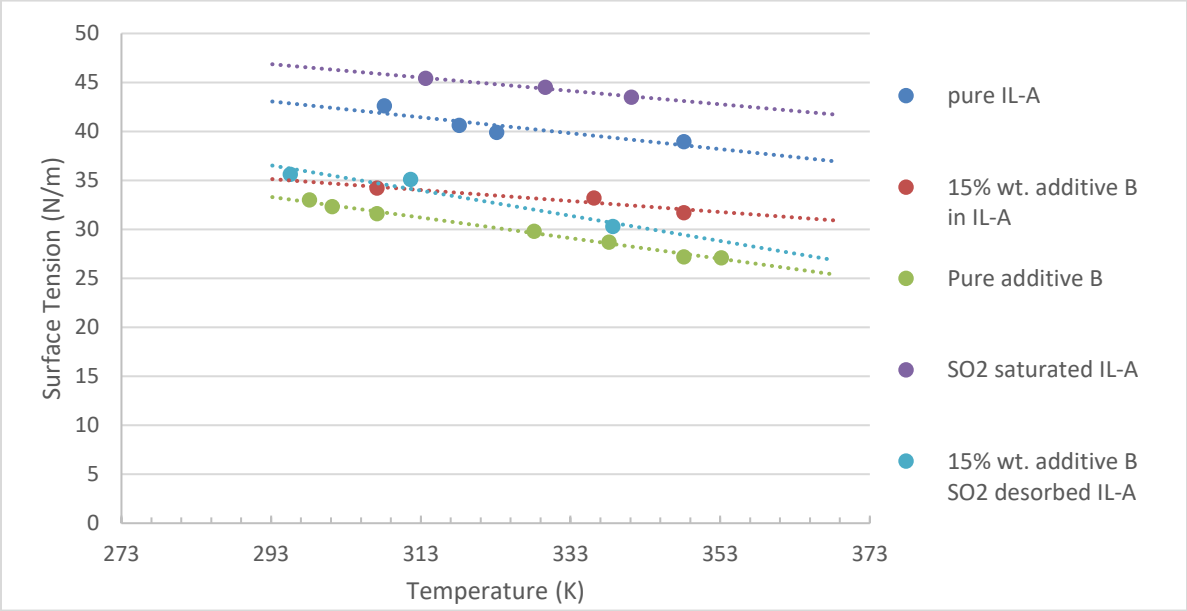

Figure 10 Effect of temperature on the surface tension of various IL-A systems

Table 2 Surface tension of liquid phases measured at different temperatures

T, ºC	IL-A	15% wt. additive-B in IL-A	Pure additive-B	SO2 saturated IL-A	15% wt. additive-B SO2 desorbed IL-A
22.4					35.6
25			33		
28			32.3		
34		34.2	31.6		

35	42.6				
38.5					35.1
40.5				45.4	
45	40.6				
50	39.9				
55			29.8		
56.5				44.5	
63		33.2			
65			28.7		
65.5					30.3
68				43.5	
75	38.96	31.7	27.2		
80			27.1		
Equation	-0.0813T +44.68	-0.0561T +36.25	-0.1052T +35.40	-0.0683T +48.22	-0.1286 +39.09T
Correlation	0.80	0.88	0.99	0.98	0.92

4.3 Density

Density tests were carried out as per the procedure mentioned in section 3.5.3. The IL-A's density is greater than the density of water and it was intuitive that SO_2 absorption will increase this value. Also, the general inverse density-temperature relationship was confirmed from the experimental results. The results are summarized in Table 3.

Additive-B addition has the opposite effect i.e. density seems to decrease upon additive-B addition; to that of SO_2 absorption. Density was observed to have changed the least upon additive-B addition among all the physical properties measured. This can be attributed to the smaller difference

between densities of IL-A and additive-B. The relationship between density and temperature can be estimated by a linear equation within the temperature range tested.

Table 3 Densities of liquid phases measured at different temperatures

T ºC	IL-A	15% wt. additive-B in IL-A	SO_2-saturated IL-A	15% wt. additive-B SO_2-desorbed IL-A	additive-B
24.8				1.226	
25	1.1461				0.98063
28		1.116			
35	1.1369				
37.5		1.11			
40					0.96636
42			1.255		
44.5				1.21	
45	1.1269				
50					0.95685
55	1.1189				
56.5			1.241		
57.5		1.094			
60					0.94732
65.2				1.195	
70					0.93772
70.5			1.234		
75		1.081			

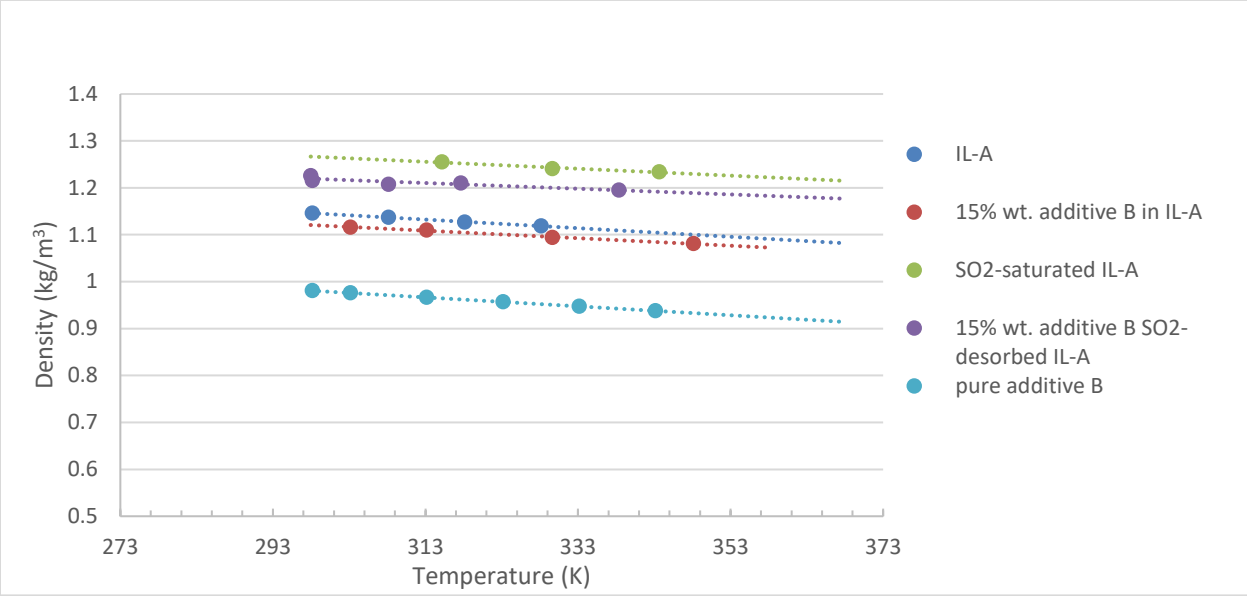

Figure 11 Effect of temperature on the densities of various IL-A systems.

4.4 Cyclic Voltammetry (CV) Experiments

The determination of the diffusivity coefficients for SO_2 in IL-A is necessary to estimate the rate of the diffusion of the gas in the solvent. These CV experiments were carried out according to the procedure described in section 3.6.

Ferrocene solutions in acetonitrile with supporting electrolyte were prepared at mentioned previously. CV experiments at 23°C were performed at scan rates of 10, 20, 50 and 100 mV/s of which 50 mV/s scan rate was used to determine the real surface area using the Randles-Sevcik equation (Randles, 1948). The diffusivity coefficient for ferrocene was taken as 2.3 x 10^{-9} m^2 s^{-1} at 298 K from the literature (Barrosse-Antle, Silvester, Aldous, Hardacre, & Compton, 2008). A typical response of Ferrocene is as shown in Figure 12.

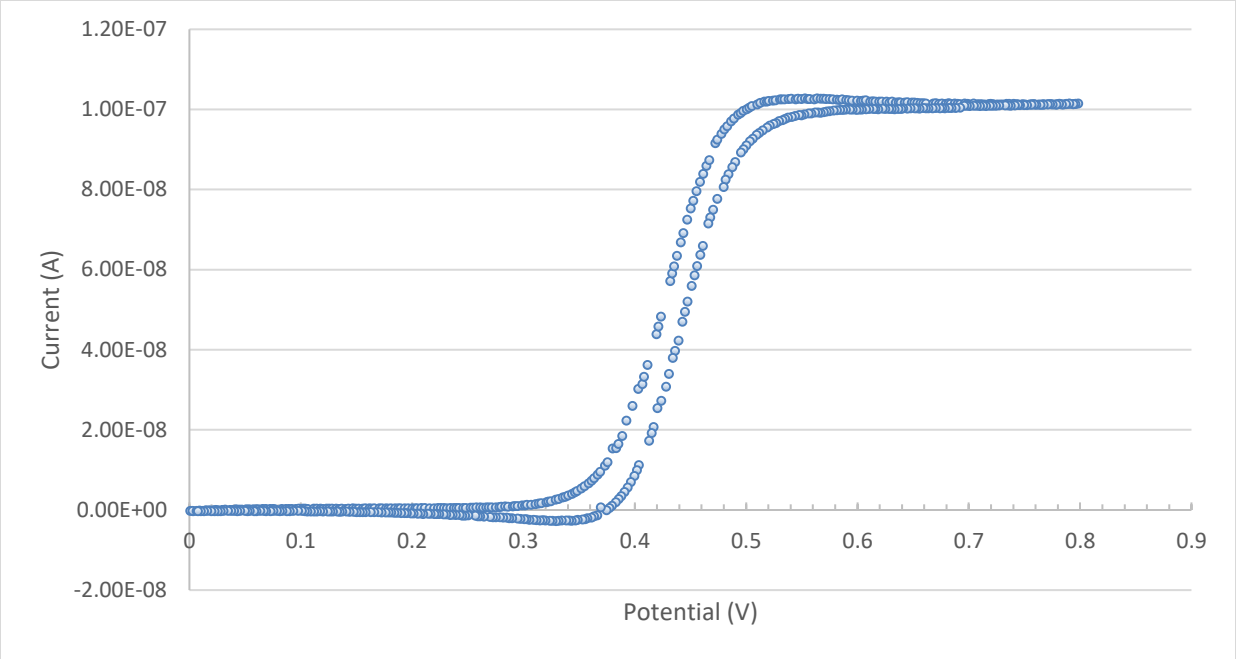

Figure 12 Response of Ferrocene for a Scan Rate of 50 mV/s

The true or effective radius of the platinum micro-disk working electrode (100 µm diameter) was found to be 147.44 µm. This value can be explained due to uneven roughness; despite of cleaning and polishing of the surface. The microbubbles formation prevents the exposure of the total surface area however it was eliminated by applying magnetic stirring before and in between the experiments.

Similarly, experiments are conducted for SO_2 saturated IL-A at 23°C with scan rates of 10, 20, 50 and 100 mV/s. Fig. shows the behavior of the saturated IL-A sample with scan rate of 50 mV/s. Peak heights of the corresponding curves at different scan rates were obtained using Origin. Using the calculated diameter and the peak height (I_p) of the 50 mV/s scan rate curve, the Randles-Sevcik equation was used to determine the diffusivity.

The Randles -sevcik equation is given as

$$i_p = 0.4463\, nFAC\left(\frac{nFvD}{RT}\right)^{\frac{1}{2}}$$

Equation 1

where, F is the Faraday's constant (C mol^{-1}), C is the concentration in mol/cm^3, D is diffusivity in cm^2/s, A is the surface area of the electrode in cm^2, R is the gas constant in J K^{-1} mol^{-1} and T is temperature in K. The parameters used are mentioned in Table 4.

Table 4 Parameters for calculating liquid phase diffusion coefficient

Parameter	Ferrocene Solution	Saturated IL-A sample
v	50 mVs^{-1}	50 mVs^{-1}
i_p	9.87 x 10-8 A	3.68 x 10-7 A
n	1	1
F	96485.33 C mol^{-1}	96485.33 C mol^{-1}
A	TBD	17.072 x 10^{-5} cm^2
R	8.31446 J K^{-1} mol^{-1}	8.31446 J K^{-1} mol^{-1}
T	296.15 K	296.15 K
D	2.3 x 10^{-5} cm^2 s^{-1}	TBD

The liquid phase diffusivity was calculated to be 1.286 x 10^{-9} m^2/s for SO_2 in IL-A.

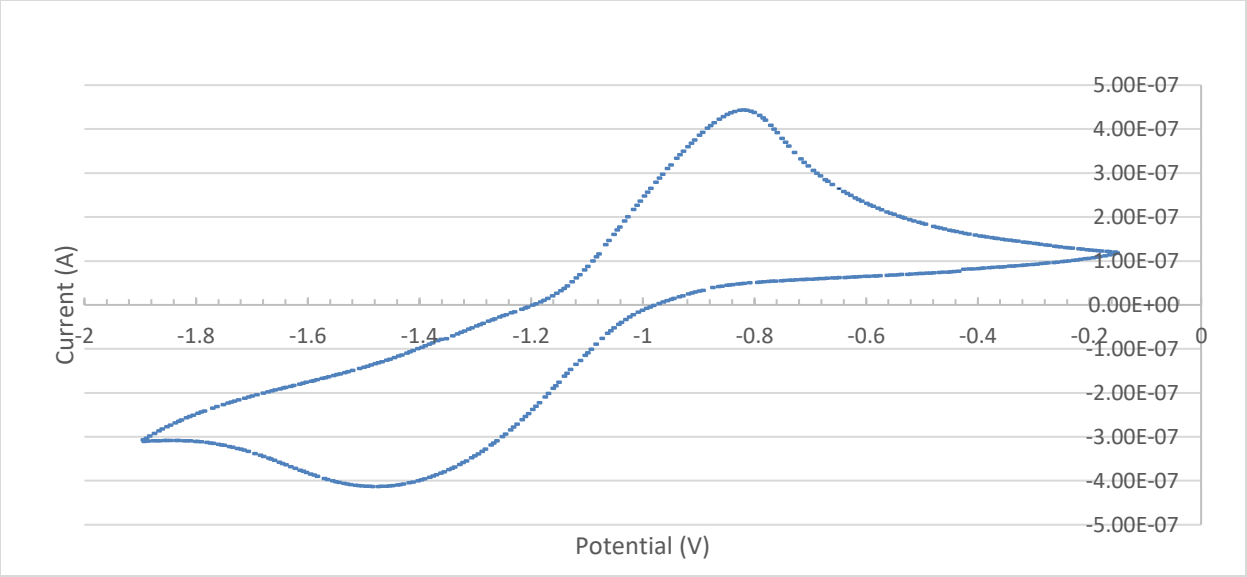

Figure 13 Typical response of IL-A for a Scan Rate of 50 mV/s

Also, the plot of i_p verses $v^{0.5}$, i.e. peak current at different scan rates (see Figure 14 Peak current versus square root of Scan Rate for IL-A-SO2 system) gives an insight of the reversibility of the reaction. If the plot is linear, the reaction is reversible and it indicates that it reaction does not cause major structural changes in the analyte. For the saturated sample, this relationship was almost linear with the correlation factor 0.97 which is in line with the reversibility property of the ionic liquid with SO_2.

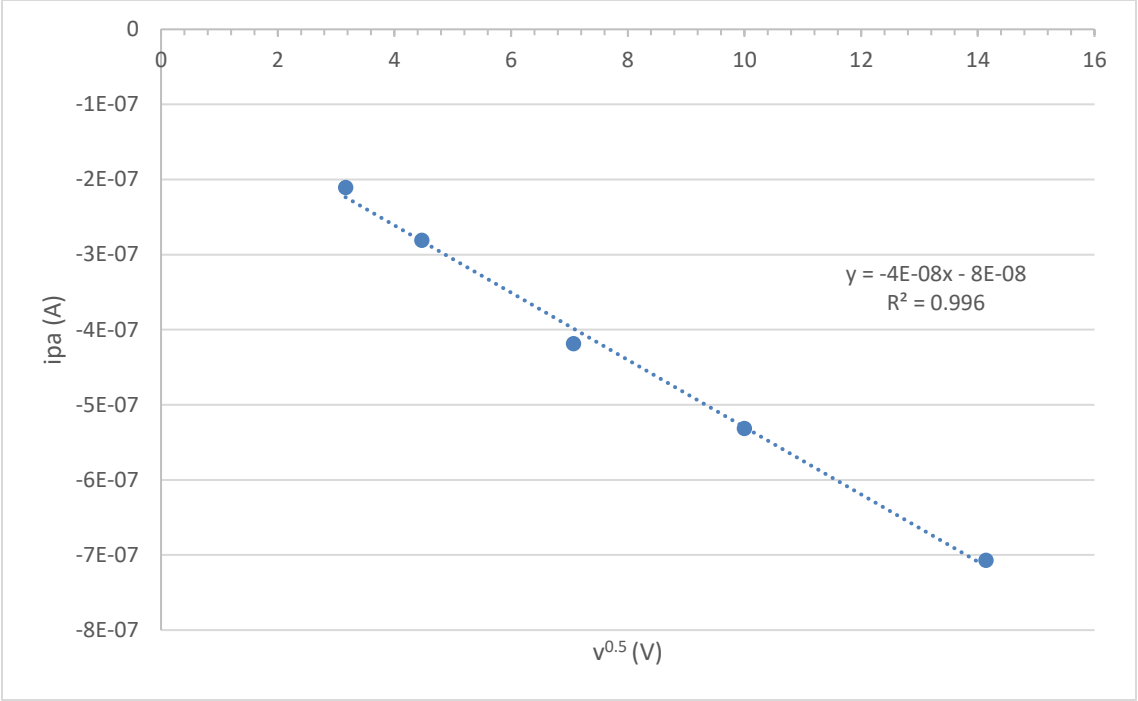

Figure 14 Peak current versus square root of Scan Rate for IL-A-SO_2 system

The gas phase diffusivity was estimated using the Fuller's method (Tang, Cox1, & Kalberer, 2014) as

$$D(A,B) = \frac{1.0868\ x\ T^{1.75}}{\left(\sqrt[3]{V_A} + \sqrt[3]{V_B}\right)^2 \sqrt{m(A,B)}}$$

Equation 2

Where D(A, B) is the diffusivity of A in B at temperature T (K), V_A and V_B are the dimensionless volumes of the two gases and are estimated from the work of (M. J. Tang et al.: Gas phase diffusion coefficients: inorganic compounds), m(A, B) is given as $m(A,B) = \frac{2}{\left(1/m_A + 1/m_B\right)}$.

The gas phase diffusivity coefficient value was calculated at 23^0C and the values for V_A and V_B were taken as 41.8 and 19.7 respectively and m(A, B) was calculated to be 40.016. At this condition, gas phase diffusivity was calculated as 1.344 x 10^{-5} m^2/s.

4.5 Moisture Content and hygroscopic nature of solvent

Moisture in the IL-A and additive-B solutions was analyzed before and after absorption as discussed in section 3.7. Experimental results are shown in Table 5 and are reproducible with a variation of ±0.05%.

From the results, it is evident that there is still some moisture present even after desorption at elevated temperatures of 65^0C. Also, the moisture content increases tremendously if the sample is exposed to the environment and this phenomenon has been observed in the works of Santiago ((Aparicio, Alcalde, & Atilhan, 2010)) for IL-A. After purging with N_2 gas at elevated temperatures for about 12 hours, the sample moisture content drops to 1.4 %. However, this pretreatment is further carried on until constant weight of the sample is obtained and is lowers to approximately 0.9-1.1% by weight.

IL-A as shown by Santiago et. al. (Aparicio, Alcalde, & Atilhan, 2010), by itself is known to be hygroscopic but, from our observation, the presence of SO_2 has an accelerated effect on it absorbing more water. A sample was taken and analyzed directly after the third cycle absorption cycle had retention moisture content of 0.6 %. Titration of the same absorbed sample stored in a very humid for 48 hours was carried out to confirm the hygroscopic nature of the IL-A+SO_2; and as per the expectation, the moisture content increased to 21%. Although, the desorbed sample showed lost significant amount of moisture over time and moisture content after 3 cycles reduces to 0.54%. It can be argued that SO_2 loosely bounds with the H_2O and at elevated temperatures, these two species are lost simultaneously. Also, and so IL-A being a basic, offers slightly alkaline medium for the reaction with SO_2 with water will result in an acidic mixture

On a side note, another interesting observation of this test was the visual decrease in viscosity of IL-A upon moisture uptake. This viscosity effect can aid as an alternative to the additive that is used as viscosity improver. However, other effects such as corrosion need to be taken in to consideration. Water has high vapor pressure hence it can be removed by maintaining the desorption temperature at elevated temperature but a new set of equipment would be needed to capture this water, to purify and recycle back to mix with IL-A.

Table 5 Moisture content in different liquid phases.

Sample	% H_2O (±0.05%)
Fresh IL-A (from bottle)	1.97 %
Fresh IL-A + additive-B (before absorption)	2.13 %
IL-A + additive-B (in pre-treatment)	1.4 %
Absorbed sample (standing after 48 hours)	21 %
IL-A immediately after third abs cycle	0.6 %
IL-A immediately after third des cycle	0.54 %

4.6 Thermogravimetric Analysis (TGA) Experiments:

TGA was performed for fresh and SO_2 absorbed IL-A to understand the vapor pressure of the IL-A and additive-B, as well as to get an estimation of the amount of solvent loss in the operating temperature range. Calibration of the equipment was performed with standards of Zinc (melting point 419.5°C) and Indium (melting point 156.61°C). The experimental temperature values were determined with these two standardized highly pure metals and then plotted against the real temperature values obtained from the experiments to get a calibration curve. The temperature values and calibration plots are as shown in Table 6 and Figure 15 respectively. The TGA behavior

of Zinc and Indium are given in the Appendix. To validate the experimental results, known boiling point of pure additive-B was checked with the experimental results and the accuracy was well within the range of $\pm 0.1^0$C.

Table 6 Table for calibration of TGA

material	Real temperature (ºC)	Experimental temperature (ºC)
Zn	419.5	405.7
In	156.61	150.93

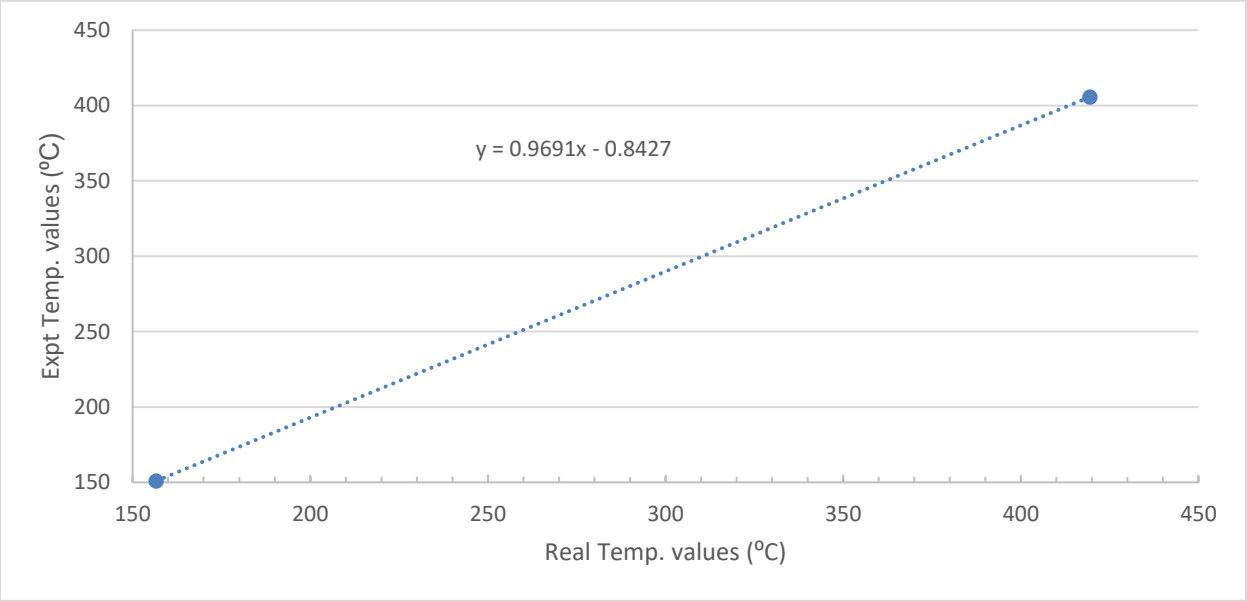

Figure 15 Calibration Chart for TGA Analysis

A Typical thermogram represents a heat flow, temperature and weight of the sample curves for the material in testing. To obtain the degradation temperature analysis of IL-A, the onset of inflection of heat flow curve was observed from its plot. It started to deflect at the temperature of 218.45ºC and was lowest at about 272.33ºC meaning all the IL-A was lost at this temperature. Degradation temperatures of other similar cation based ionic liquids from literature are also in the vicinity of

300°C. ((Ngo, LeCompte, Hargens, & McEwen, 2000)). An isothermal 10°C step TGA at slow scanning rate for IL-A was performed in the temperature range of 25 to 85°C to estimate the amount of solvent loss in the process operating range (Figure 16). Over the course of 22 hours, 1.52 mg (3.336 mass %) of IL-A was lost of the total 45.56 mg taken initially. Arguably, this 3.336% contains the volatile materials and moisture present in the IL-A indicating that the net loss of the solvent is much less of about 0.5-1% by weight; considering the loss of most of moisture (~ 2-2.5% moisture and other volatile materials).

In order to validate the calibration and TGA results, the boiling point of additive-B was determined experimentally using TGA and was found to be 275.02°C which is the same as its theoretical value (275-276°C) as found in its Material Safety Data Sheet (CAS no. 143-24-8). Isothermal step TGA at slow scanning rate for additive-B in the temperature range of 25 to 85 °C (Figure 17) estimated a loss of 3.975 mg (9.45 wt %) of the total 41.93 mg taken initially. It was observed that 2.287 mg (57.54 wt %) of the total weight loss was in the temperature range of 65 to 85°C. So, if the desorption temperature is limited to 65^0C, then additive-B can still be used as the total % wt loss in range of 25-65 °C for it is less than 4 wt% considering the fact that it is very economical and essential to improve the viscosity. Alternatively, an additive-B trapping unit can be installed to recover it from the exhaust gas stream provided that it proves to be economical to operate.

TGA of the sample after 3 absorption-desorption cycles at 25 and 65°C respectively was analyzed while ramping the temperature from 25 – 500°C and the weight loss was monitored just before the onset of degradation temperature of IL-A. From the figures(appendix), the weight loss was 3.944 mg (10.41 wt %) of the total 37.873 mg of sample taken initially. This weight loss is due to loss in bounded SO_2, moisture, additive-B and IL-A. Though it is difficult to quantify the exact amount of each component of the weight loss, from the previous results with individual components, it

was suspected that most of it can be assigned to loss of additive-B. To confirm this, another sample was prepared but the desorption temperature was lowered down to 45°C. Since more of the additive-B is retained in the sample, the weight loss, as expected was higher; 7.699 mg (16.23 wt %) of the total 47.441 mg taken.

The weight loss from TGA for additive-B in the range of 45 to 75°C is 4.698 wt % which is almost equivalent to the increased weight loss in the sample 2. Thus, it which further strengthen the previous assumption that most of the weight loss is due to additive-B and hence, in order to continue using additive-B as an additive, desorption temperature should be lowered at least below 70°C. Also, the total weight loss from diluent, moisture and volatile materials constitute the majority and so making it safe to speculate that the amount of bounded SO_2 (that cannot be feasibly desorbed and is chemically bounded to IL-A) is much less in comparison to that of additive-B. Since the vapor pressure of IL-A is very low, there is no need of having an additional solvent trapping step in the process design.

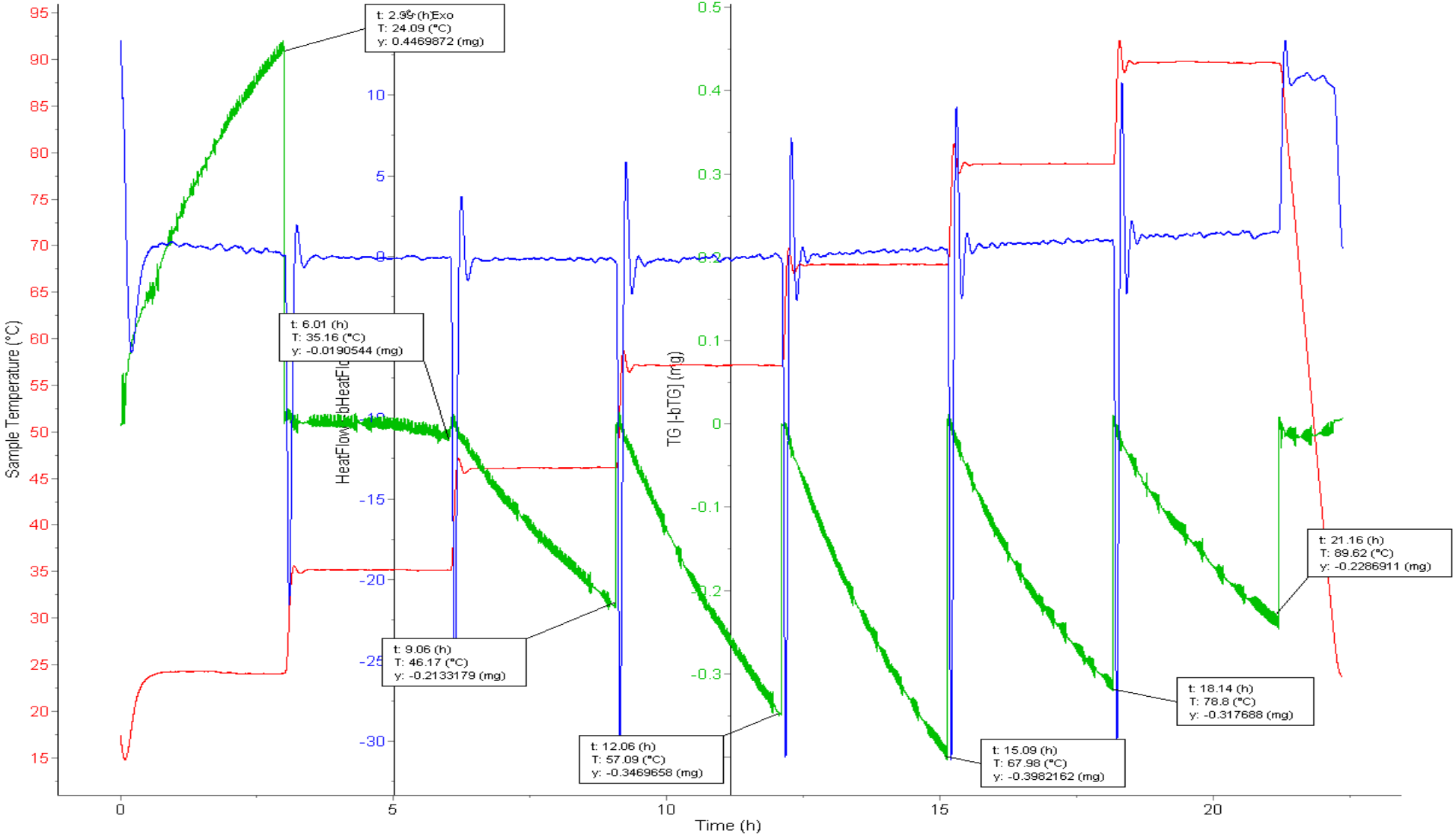

Figure 16 TGA for IL-A using low scan rate for temperature range of 25^0C-85^0C

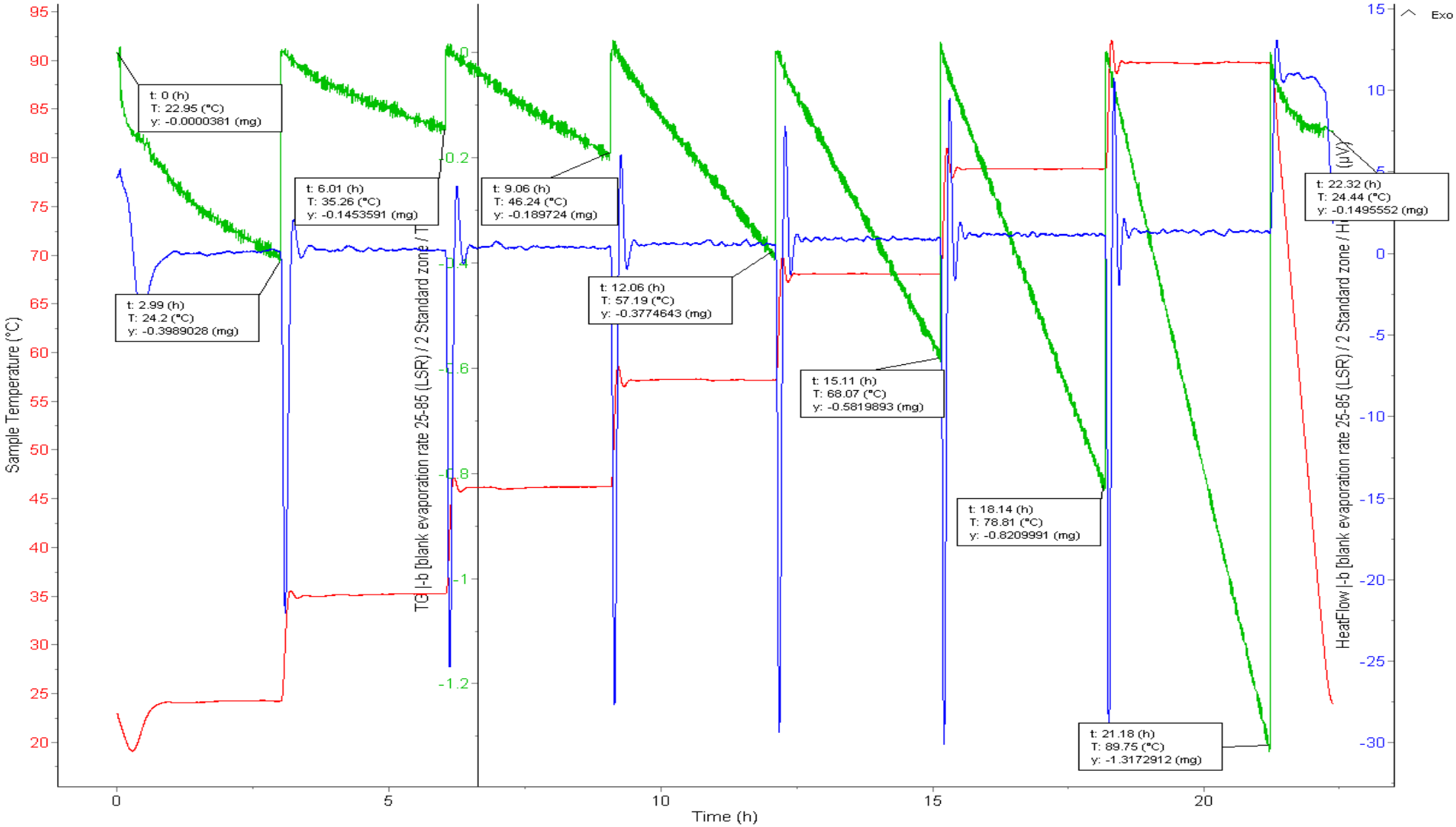

Figure 17 TGA for additive-B using low scan rate for temperature range of 25^{0}C-85^{0}C

4.7 FTIR:

FTIR was performed to analyze the SO_2-IL-A system behavior and to get an insight on the mechanism of absorption-desorption. Also, since the loss of additive-B is high, these experiments will give an estimate of the quantitative presence of additive-B before and after the absorption/desorption process. The most prominent peaks of the fresh IL-A (1593 cm^{-1} and 1115.89 cm^{-1}) and additive-B (1088.5 cm^{-1}) obtained by analyzing fresh samples from the bottle were used to make comparison all along. It should be noted clearly that there are some minor shifts in the peaks (< 10 cm^{-1}) for subsequent tests spectra which can be due to unavoidable interferences but the results were reproducible in nature.

A study by Vitor et. al. (Paschoal, Faria, & Ribeiro, 2017) on spectroscopic vibrations of IL-A cation shows that the signal in the range 2800 – 3200 cm^{-1} is assigned to CH bond stretching mode of alkyl chain attached to and of the imidazolium rings. Also, characteristic bands of ring are represented by the signals in the range 800-1600 cm^{-1}. Since this band remains unchanged in both before and after absorption spectra as shown in Figure 18 and Figure 19, it is expected that IL-A cation is unchanged and it indicates that SO_2 attaches to some site in the anion IL-A.

Santiago et. al. (Aparicio, Alcalde, & Atilhan, 2010) mentioned that the wide band that peaks at 3360 cm^{-1} is assigned to OH stretching and at 1593 cm^{-1} was due to asymmetric vibration of COO^- group of the IL-A anion. The spectra show not much change for OH stretching band but the absorbance at 1593 cm^{-1} is significantly reduced. The interaction of SO_2 with the strong-base IL-A anion of IL-A is commonly believed to be the mechanism for SO_2 absorption.

Comparison of spectra of IL-A before and after absorption at 1800 ppm concentration (fig.18) shows a newer band signal at 951.14 cm^{-1} which could be assigned to SO_3^{2-} (Brown & Straughan,

1972). A study by Li et. al. (Li, Zhang, Zheng, & Zheng, 2015) shows that this signal corresponds to antisymmetric and symmetric stretching and similar band after absorption of EMI-Acetate with SO_2 was observed at 961 cm^{-1}. However, with different Ionic liquids, the band shifts slightly due to different cationic and anionic interactions and influences. As evidenced by the FTIR spectra, SO_2 in aqueous IL-A solution is not tightly bound to the strong base anion (IL-A) of the ionic liquid but behaves like the SO_3^{2-} anion in solution.

Spectra comparison of 2 cyclic samples absorbed at 25°C and desorbed at 65 and 45°C are shown in Figure 19. It was evident that the additive-B peak at 1088.5 cm^{-1} in comparison to its adjacent IL-A peak at 1115.89 cm^{-1} showed lower absorbance in sample desorbed at 65°C. So, it indicates quantitively less amount of additive-B presence in the sample desorbed at 65°C than at 45°C. Also, the peak height of SO_2 band at 951.14 cm^{-1} was greater for the sample desorbed at 45°C than at 65°C indicating greater presence of the SO_2 in the sample. However, the IL-A cation band at 2800-3200 cm^{-1} and IL-A at 3360 cm^{-1} shows no visible changes in both samples which confirms that SO_2 is attached to the anion IL-A.

To estimate the amount of additive-B present after 3 cycles for the 65°C desorption sample, it was compared with spectra of IL-A with different amount of the additive, as seen in Figure 20. Though this is not much accurate, as the interaction of additive-B with SO_2 was not taken in to consideration, it was good enough to give a perspective of the amount of additive-B lost and can be taken as a semi-quantitative for comparing relative values. A visual comparison can be made for the SO_2 peak in all the samples. The peak at 1088.5 cm^{-1} was highest for the sample with 20% additive-B sample and was lowest for sample with 5% additive-B. By analyzing the spectra for sample desorbed at 65°C, additive-B after 3 cycles was slightly greater than 5% by weight and about 9% of the additive-B was lost during the operation.

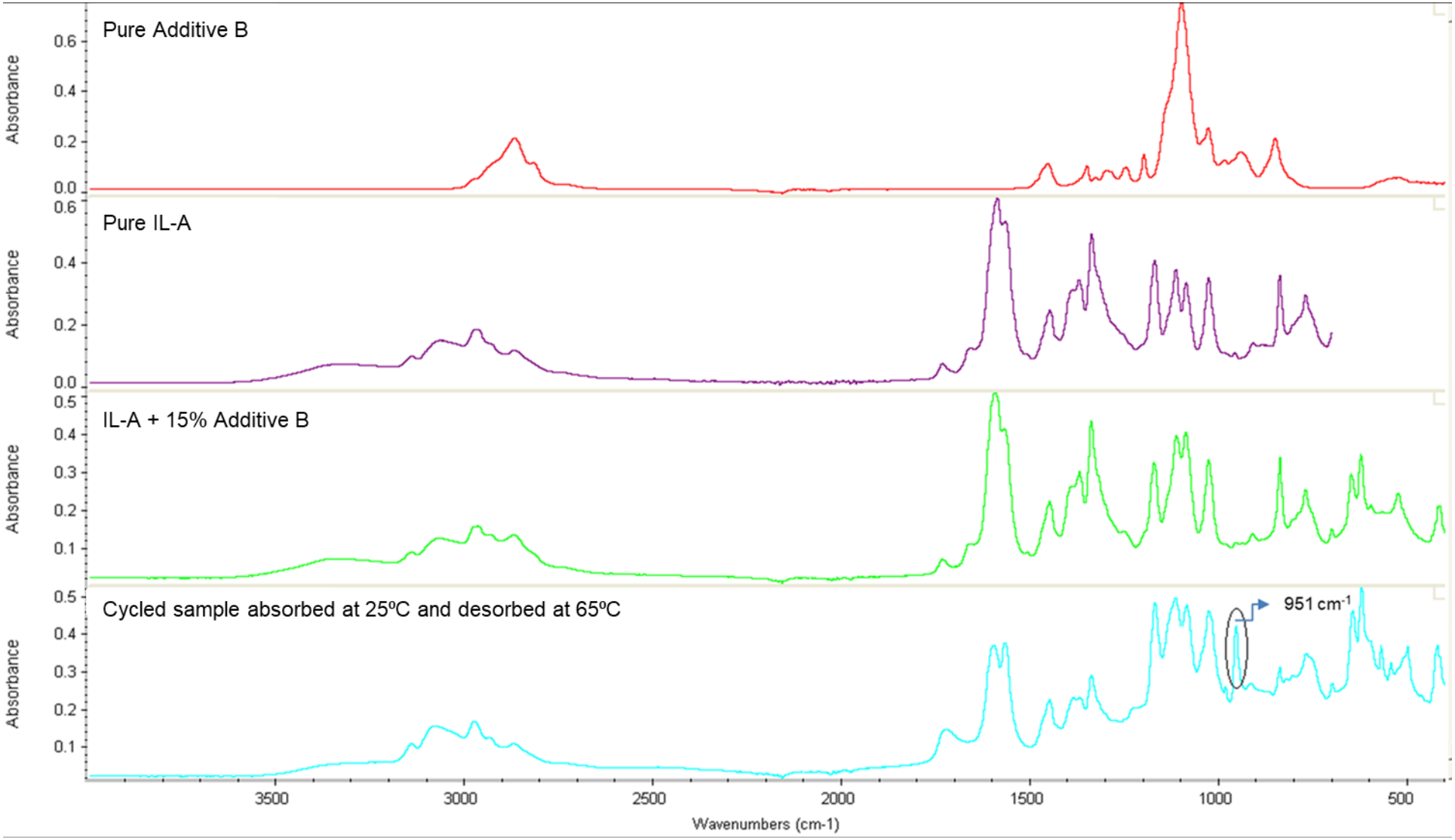

Figure 18 FTIR response of Fresh ionic liquid, fresh additive, its mixture and after 3 cycles of absorption - desorption

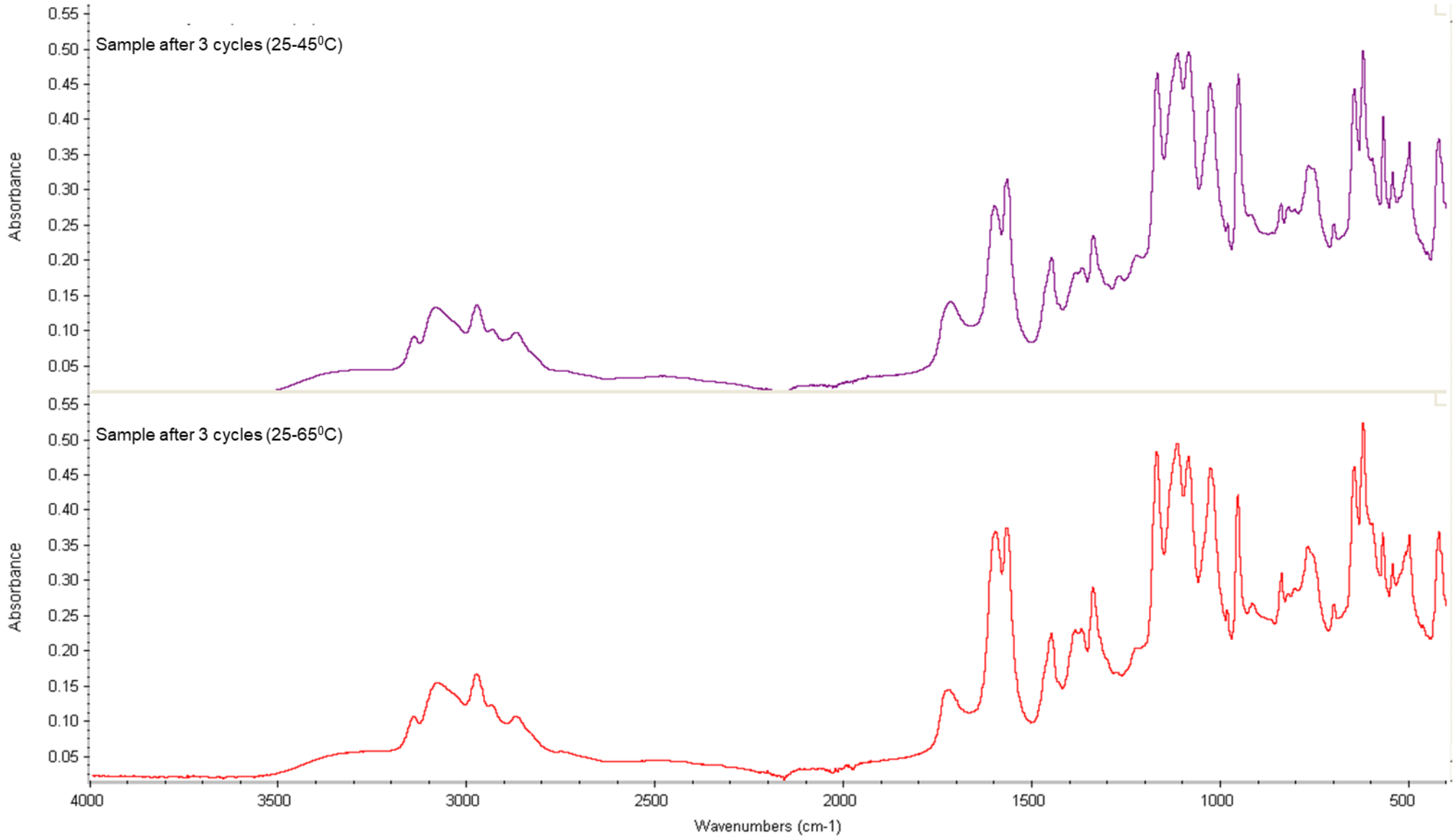

Figure 19 FTIR comparison of cycled samples absorbed at 25^{0}C and desorbed at 45^{0}C and 65^{0}C

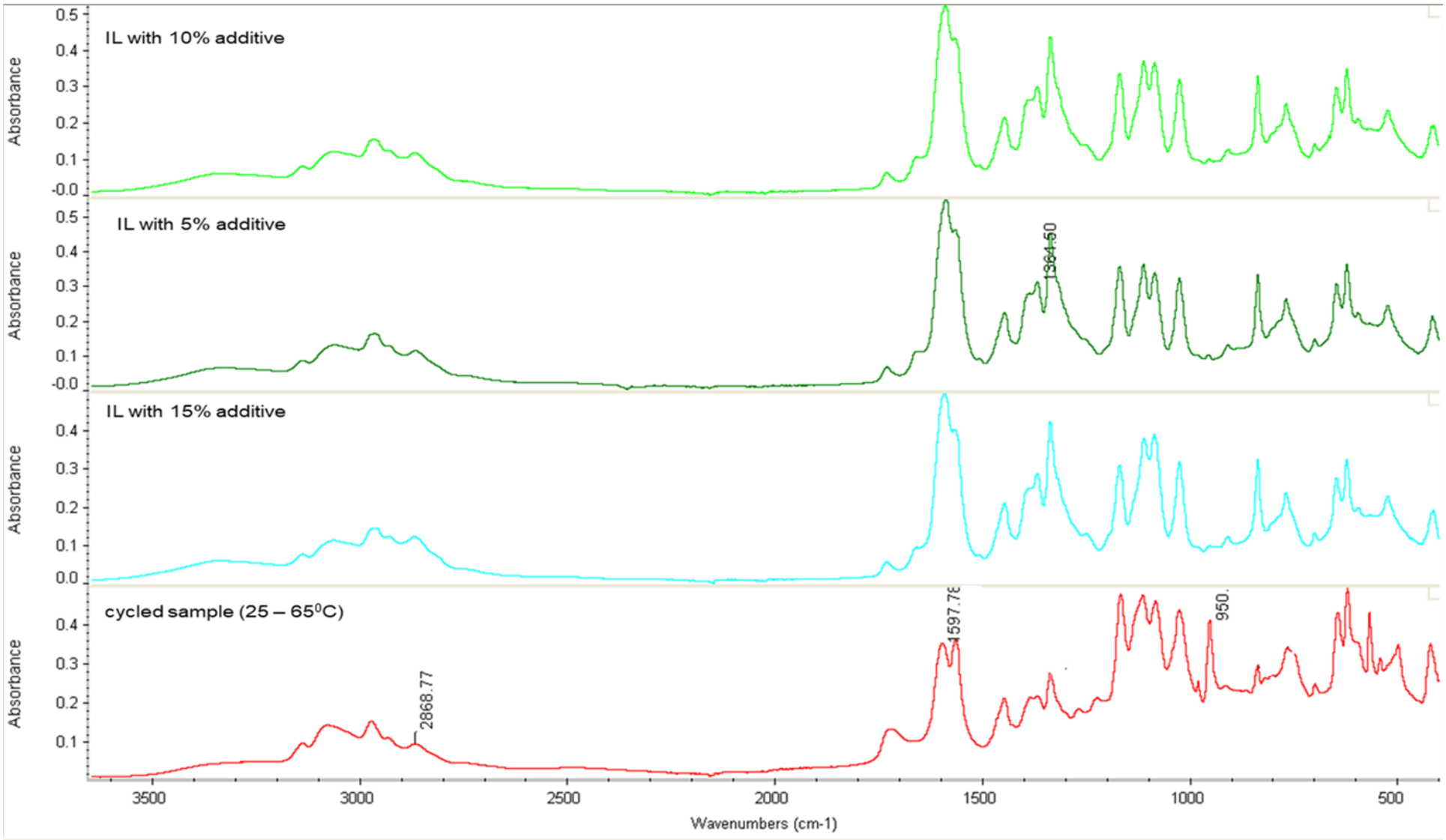

Figure 20 Comparison of FTIR for ionic liquids with different amount of additive

Chapter 5

TOWER DESIGN CALCULATIONS

5.1 Gas-Liquid Equilibrium Data:

Equilibrium experiments with IL-A and 1800 ppm SO_2 were conducted for this project to get appropriate equilibrium data and to obtain a starting point for the tower design calculations. No such equilibrium data were found for the IL-A-SO_2 system in the literature to the best of our knowledge. Since it was soon discovered that viscosity improver additive-B needs to be added, the equilibrium data shown here are limited to IL-A containing 15% additive-B and the experimental procedure is followed as discussed in section 3.3 and below.

Equilibrium experiments were too time consuming to be performed at all required temperatures and pressures. So, 3 temperatures were chosen for each of these cycles and then extrapolated using Vant Hoff's equation to determine the equilibrium mole fraction of SO_2 in ionic liquid at the temperatures of choice. Absorption experiments were carried out at 35 ºC and the same saturated sample was desorbed at 35 ºC using a pure N_2 stream, whereas the sample absorbed at 25 ºC was first desorbed at 25 ºC and then it was continued to be desorbed at 45 ºC to save time before conducting absorption experiments on the regenerated IL. A similar sample was absorbed at 65 ºC but during its desorption at 65ºC, due to experimental failure of the flow controller and excessive foaming, a small amount of sample was lost in to the scrubber and hence desorption at 65 ºC was not taken into consideration in this report.

The Van't Hoff's - Henry's law relationship with temperature is represented as shown in equation Equation 3.

$$\frac{d\ lnK_{eq}}{d(1/T)} = \frac{-\Delta_{sol}H}{R}$$

Equation 3

Where, $\Delta_{sol}H$ is the dissolution enthalpy, which does not change much with the temperature in the range of temperature considered here. K_{eq} is the equilibrium concentration of product/reactant. Here, the concentration of SO_2 in the gas phase is constant at 1800 ppm, K_{eq} varies only with respect to equilibrium conversion, X_{SO2}. So, a plot lnX_{SO2} vs. 1/T instead of lnK_{eq} vs. 1/T can be drawn. The absorption and desorption plots are shown in the Figure 21 and Figure 22.

The plots in Figures 21 and 22 show linear relationships, as trendline linear fit curve gives the equation $lnXso_2$ = 1347.8(1/T) - 5.584 with R-squared value of 0.999. Similarly, the trendline linear fit curve gives the equation $lnXso_2$ = 2879.4(1/T) - 11.284 with R-squared value of 0.989 for desorption. These linear fits are consistent with the low concentration solute-solvent dilute system and will follow Henry's law. Though the desorption was carried out using N_2 purging, similar data is expected to be replicated using Vacuum desorption. The focus in this research project was on SO_2 absorption by IL. From the above relationships, the mole fractions at other temperatures can be easily determined. Table 7 Equilibrium mole fraction of SO2 in Solvent at various temperatures summarizes the results for the mole fraction of SO_2 in the solvent obtained at different temperatures and after both absorption and desorption. As the temperature increases the equilibrium mole fraction of SO_2 in the solvent decreases which follows the general gas solubility rule. For the desorption operating temperature of 75ºC, 0.049 mole fraction of SO_2 is retained in the solvent stream indicating permanent loss of equivalent capacity in the following cycle.

For dilute solution system such as the one in consideration, equilibrium solubility line represented by Henry's law is straight and its slope represents the Henry's law constant. Henry's law is represented as $y_A = m\ x_A$, where y_A and x_A are the equilibrium mole fraction in gas phase and liquid phase and m is the Henry's constant. Since in the experiments, y_A was fixed to 1800 ppm and x_A was determined from the Vant Hoff's relationship, m, the slope of the equilibrium line can also be estimated. The operating curve for absorption lies above the equilibrium line whereas the desorption/stripping has its operating curves below the equilibrium for a feasible system (Fair, Steinmeyer, Penney, & Crocker).

Table 7 Equilibrium mole fraction of SO_2 in Solvent at various temperatures

Temperature (^oC)	**Process**	**Equilibrium Mole fraction of SO_2 in ionic liquid (Xso2)**
25	Absorption	0.347
	Desorption	0.193
35	Absorption	0.295
	Desorption	0.149
45	Absorption**	0.259
	Desorption	0.105
65	Absorption	0.202
	Desorption**	0.063
75	Absorption**	0.180
	Desorption**	0.049

** values are estimated based on the vant hoff's plot.

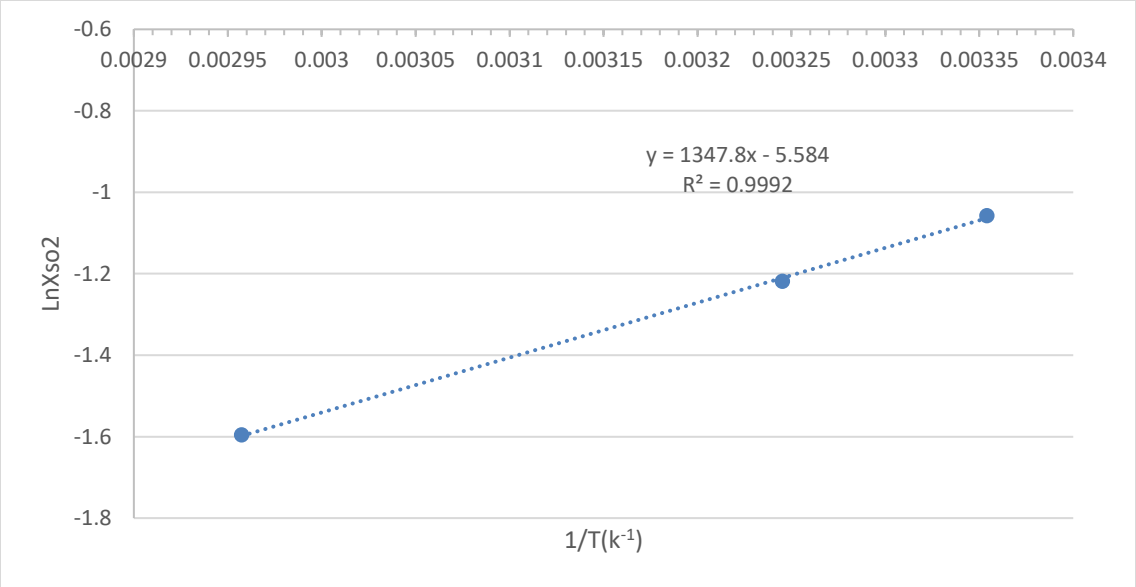

Figure 21 lnX_{SO2} versus 1/T plot for absorption

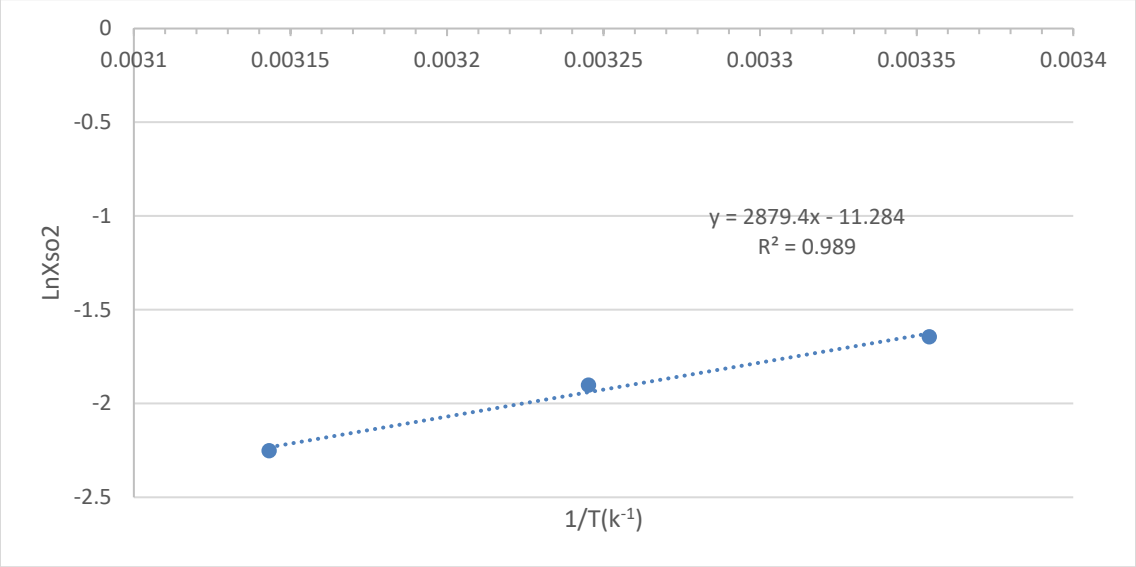

Figure 22 lnX_{SO2} versus 1/T plot for desorption

5.2 Cyclic Experiments:

As seen in Table 7, the equilibrium experiments indicated that not all the absorbed SO_2 was getting desorbed. This indicated that the part of SO_2 reacts with IL-A and gets permanently absorbed depreciating the capacity of the IL-A over each cycle. However, since the absorption-desorption

was carried out at same temperatures, it was inevitable to perform them at process conditions to get better insights on the absorption capacity loss. Cyclic experiments were conducted with two samples of 2 g, both at absorption temperature of 25 ºC. The desorption temperature was at 65 ºC for sample 1 and 45 ºC for sample 2. Since there is no predetermined method of analyzing SO_2 in ionic liquids, the weight change of the sample after absorption and desorption were used to estimate the behavior over different cycles for SO_2 loading in IL-A. The results are presented in Figure 23.

The first observation regarding cycling samples was that foaming was more intense at 65 ºC desorption as compared to 45ºC. This can be explained by the fact that surface tension decreases at elevated temperatures. Also, foaming seems to dampen with the subsequent cycles however it is not significant relative to its initial cycles.

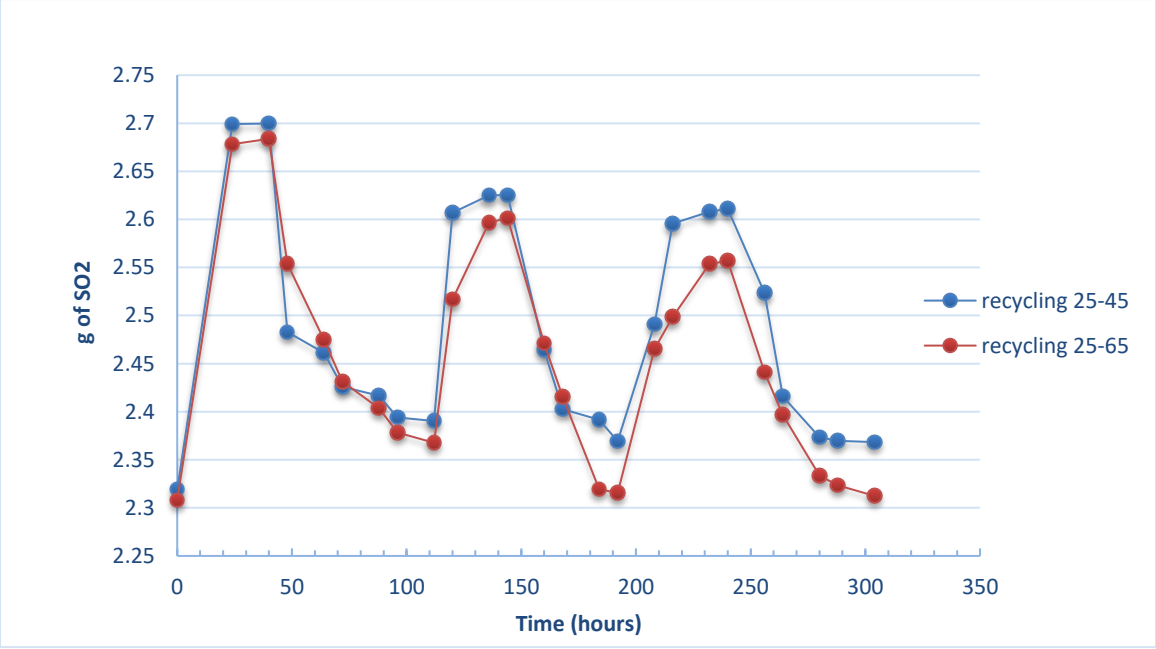

Figure 23 recycled Samples with absorption at 25^{0}C and desorption at 45^{0}C and 65^{0}C.

Absorption in the first cycle for fresh samples 1 and 2 was about 16.42 wt.% and 16.28 wt.%, respectively, which is consistent with the equilibrium results obtained in Table 7. In the subsequent

cycles, the absorption decreases to 10.45 wt.% and 10.73 wt.% by wt. in the second and third cycles for both samples. During desorption of sample 1, total weight loss in the first cycle was 13.34% desorbed which suggest that at least 3.07% by wt. of absorbed SO_2 was not recoverable. Also, the total weight loss does include the loss of additive-B. In the 2nd and 3rd cycle, the total weight loss was 11.38 wt.% and 10.97 wt.%, respectively, for desorption at 45 ºC (sample 2), whereas the total weight loss for desorption at 65ºC (sample 1) was higher at 12.78 wt.% and 10.92 wt.% for 2nd and 3rd cycle, respectively. However, this weight loss account for loss in additive-B, SO_2 and minute quantity of water. This loss of additive-B and water was confirmed in FTIR and Karl Fischer titration respectively, as discussed in sections 4.4 - 4.6.

These experiments highlight the fact that there is capacity loss of IL-A due to permanent absorption of SO_2 and fresh IL needs to be added as it will be exhausted progressively. Also, additive-B as an additive is lost at a faster rate and which makes the abs-des process slower with each progressing cycles. So, similar other additive should be considered; as an alternative, vacuum desorption could be considered to avoid excessive losses.

5.3 Preliminary Selection of Gas-Liquid Reactor

It is important to find a compact reactor which could effectively capture SO_X from marine engine flue gas. Conventional industrial methods to capture CO_2 or SO_X employ various gas absorption devices. In these devices, gas–liquid contact is achieved by dispersing the gas phase in the liquid phase to obtain large contact areas, thus increasing the mass transfer rate. Even though these contact methods are very popular in industry, they are more commonly used for water type liquids and the design could be different with viscous ionic liquids.

For SO_2 absorption and desorption with IL liquids, there is no such practice. Each reactor has its unique features. Through reviewing various gas-liquid reactors, one can better understand the

impact of the reactor type and design, which guides bench-top scale gas-IL reactor`s selection and design. Many types of gas-liquid reactors have been developed for gas absorption. These include bubble columns, packed bed columns, trickle beds, plate or tray columns, spray columns, wiped film, spinning film reactors, stirred vessels, plunging jet, surface aerator, static mixers, ejectors, venturi and orifice plates, three-phase fluidized bed, and novel hollow fiber ceramic contactors. Although varied from reactor to reactor, the selection of reactor type is generally dictated by the following factors:

- viscosity;
- gas-liquid mass transfer regime;
- flow pattern;
- retention time;
- foaming properties; and,
- other constraints, like presence of particulate matter (PMs), heat transfer and properties of materials.

Of all the possible choices, packed tower design offers considerably greater advantages of those mentioned above for dilute gas solvent systems over other designs. The next section explores further on the selection of packed tower design.

Packed Tower/Packed Bed Reactors

Packed tower is a most common apparatus used in gas absorption. An example of a packed tower is shown in Figure 24. The device consists of a packing bed, a gas distributor, a liquid distributor, packing materials, packing support plate, and a mist eliminator.

The inlet liquid is distributed over the top of the packing by a liquid distributor and uniformly wets the surfaces of the packing. The flue gas enters the distributing space from below and flows upward

through the interstices in the packing. The packing provides a large area of contact between liquid and gas, and enhances intimate contact between G/L phases. At steady state conditions, for specified flow rates of liquid and gas phases, the extent of absorption will reach equilibrium. The packing tower can be designed for recycled or single-use liquids, depending upon process conditions.

Packed-bed reactors have the advantage of counter-current flow, low pressure drop and a wide range of available materials for construction. They can be designed for high or low gas/liquid ratios. The key to designing a packed column for gas absorption is the tower packing, where the pressure drop should be minimized, while still maintaining a high surface area where the absorption of the gas occurs. The type of packing most suitable for any application will vary with temperature, pressure, gas concentration, and efficiency requirements. Careful consideration is given to various alternatives before selecting the packing for each application. Packing materials selection will be addressed in the calculation of the tower.

A packed bed reactor could be a good option for ionic liquid-SO_2 absorption. In view of the high viscosity of the IL absorbent, many parameters, such as mass transfer coefficient, flow pattern, gas and liquid flow rates, etc., need to be determined through experiments and/or modelling.

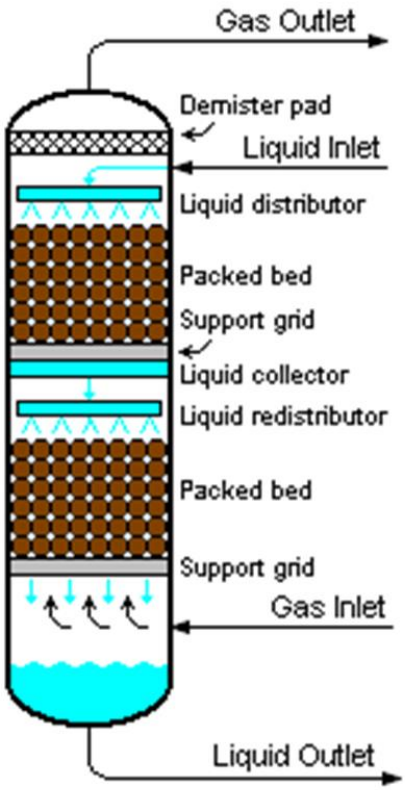

Figure 24 Example of a packed tower reactor

5.4 Scale-Up Design Projection:

In order to draw a comparison in terms of size and compactness of this tower with that of commercial wet scrubber, an industrial 20MW marine diesel engine wet scrubber was benchmarked for comparison. A 20MW wet scrubber scrubs about 61,600,000 L/hr. of flue gas and has an approximate dimension of 4.6 m diameter and 9.0 m in height. For IL-A as a solvent to make sense, tower footprints should at least be of same or lesser than benchmark scrubber. Much of the space requirement is already reduced due to minimal waste storage requirement owing to recyclability of the solvent. On the other hand, a new desorption tower needs to be added which offsets the space reduction advantage. The temperatures of absorption and desorption for the

design here will be set to 25ºC and 75ºC respectively. However, a larger temperature difference between the absorption and desorption towers will lead to a more efficient process.

Equilibrium experiment data were used to calculate the equilibrium SO_2 concentration in the solvent at design temperatures. The physical properties data were used as determined experimentally from Chapter 4. The flue gas emission flow rate and scrubber area of a typical 20MW engine were taken as $61.6x10^6$ L/hr. and 18.4 m^2, respectively, and were used as a benchmark for comparing HTU. The minimum liquid flow rate, on the other hand, was based on mass balance—i.e., the amount IL-A needed to absorb SO_2 down to required performance specification. IMO regulations were used as required reactor performance specification (i.e., 1800 ppm SO_2 in and 50 ppm SO_2 out). The reactor design modelling was based on the method described in the book of Billet and Schultes (R.Billet & M.Schultes, 1999). The correlations and design calculations procedure for tower design are discussed next. Thereafter, the names scrubber and absorber have been used inter-changeably.

5.5 Absorber Tower Calculations:

For designing a packed tower for absorption of dilute gases, several assumptions can be made to get the preliminary tower design due to lack of available literature and experimental data. For this dilute gas absorption system, the equilibrium and operating lines are regarded as straight line and the equation of operating line can be taken as

$$G'(y_1 - y_2) = L'(x_1 - x_2) \qquad \text{i.e.} \qquad x_1 = G'/L'\,(y_1 - y_2) + x_2$$

Equation 4

The equilibrium line is drawn based on the experimental values as mentioned above. Also, the gas rate (G') and liquid rate (L') over the height of packings remain constant. It was evident that not

all of the SO_2 is removed and from desorption equilibrium data, at 75°C about 0.049 mole fraction of SO_2 (Table 7) is retained in the solvent. Since the rate of desorption slows down after about 0.063 (Table 7) mole fraction, it seems more feasible and time efficient to design tower with recycled solvent stream containing roughly 0.0627 SO_2 mole fraction. Table 8 and figure 25 indicate the mole fractions of SO_2 in solvent stream entering and exiting the absorber tower.

Table 8 The equilibrium and operating SO_2 mole fraction in solvent and gas phase.

Absorption	**Yso2**	**Xso2**
equilibrium line	0	0
	0.0018	0.3474
operating line	0.0005	0.0627
	0.0018	0.30

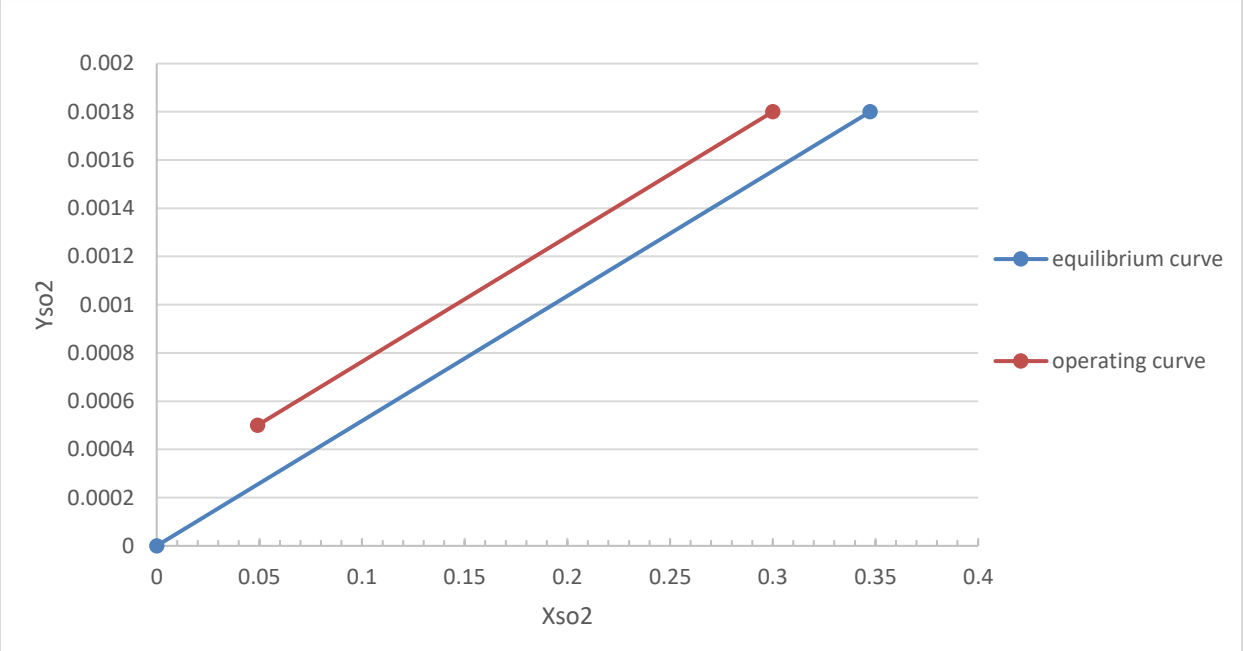

Figure 25 operating and equilibrium line plot for absorption tower design.

Problem statement:

SO_2 is to be absorbed by 85% IL-A and 15% additive-B solution from a flue gas stream containing 1800 ppm SO_2 using a packed tower on initial unit cross-sectional area. Subsequently, the cross-sectional area was modified to analyze its effect on tower height. Since the SO_2 outlet target is 50 ppm, 97.22% of SO_2 needs to be removed. The feed gas rate is 72.9 x 10^3 kg/hr. The absorption temperature is 35 ˚C (308.15 K) and pressure is 101.325 kPa. The height of the packing unit can be calculated as below.

Overall height (Z) of the packing unit is given by a simple equation;

$$Z = H_{oG} * N_{oG}$$

Equation 5

5.5.1 Calculation of Number of Transfer Units

Number of Transfer units (N_{oG}) is the measure of the difficulty of the separation. This value can be estimated by Equation 6.

$$N_{oG} = \int_{y2}^{y1} \frac{(1-y)_M^* \, dy}{(1-y)(y-y^*)}$$

Equation 6

Since, both operating and equilibrium lines are straight, according to method described in Coulson & Richardson's Chemical engineering hand book (Sinnott, 1993), the number of transfer units depends only on the ratio of mole fraction of SO_2 before and after absorption and on the molar flow rates of gas and liquid phases. The simplified equation for number of transfer units can be given as

$$N_{OG} = \frac{1}{1-\left(\frac{mG_m}{L_m}\right)} ln \left[\left(1-\frac{mG_m}{L_m}\right)\frac{y_1}{y_2} + \frac{mG_m}{L_m}\right]$$

Equation 7

Average molecular weight of gas phase is 0.0018(64.07) + 0.9982(28.96) = 29.02 g/mol

Molar flow rate of gas entering the tower = 2514 kmol/hr-m^2

SO_2 entering the tower is 2513.598 kmol/hr-m^2 x 0.0018 = 4.524 kmol/hr-m^2

SO_2 absorbed in the tower is 4.524 kmol/hr-m^2 x 0.972 = 4.398 kmol/hr-m^2

SO_2 leaving the tower is 4.524 - 4.398 = 0.125 kmol/hr-m^2

So, total gas leaving the absorption tower is 2509 kmol/hr-m^2

Mole fraction of SO_2 in exit gas (y_2) is 0.1257/2509 = 5.01×10^{-5}

Mole fraction of SO_2 in entering flue gas (y_1) is = 1.8×10^{-3}

The minimum amount of solvent required based on overall material balance can be determined as:

$$G'(y1 - y2) = L_{min}'(x1 - x2)$$

Equation 8

So, $L_{min}' = 18.540 \frac{kmol}{hr\ m^2}$.

Taking a factor of 2, actual molar flowrate of solvent stream $L' = 37.08 \frac{kmol}{hr\ m^2}$.

Now, N_{OG} is calculated using the equation Equation 7.

Therefore, N_{OG} for a tower was determined to be **4.868.**

5.5.2 Calculation of Height of Transfer Units

Billet and Schultz have published various correlations and constants for about 70 different types of packings of various sizes and materials. To select the best packing for most economical packed

tower design, HTU calculations is done for all the packings for which relevant data are available. These iterative calculations are performed in MATLAB (see Appendix C for the MATLAB code). The relationship between the overall height of transfer unit and individual film transfer coefficient is given as

$$H_{OG} = H_G + \frac{mG_m}{L_m} H_L \qquad \text{or} \qquad H_{OL} = H_L + \frac{L_m}{mG_m} H_G$$

Equation 9

For H_{OG} calculations, there are various correlations published based on different types of packing materials. However, since we are carrying out a preliminary design work, Onda's method (Kakusaburo Onda, 1968) is taken in consideration for the Height of the Transfer Unit calculations shown here. This method gives correlations for the gas (K_G) and liquid (K_L) film transfer coefficients and effective packing area (a_w) and these are useful to calculate H_G and H_L.

The effective packing area can be calculated as per the equation given below.

$$\frac{a_w}{a} = 1 - \exp\left[-1.45\left(\frac{\sigma_C}{\sigma_L}\right)^{0.75}\left(\frac{L_w}{a\mu_L}\right)^{0.1}\left(\frac{L_w^2 a}{g\rho_L^2}\right)^{-0.05}\left(\frac{L_w^2}{\sigma_L \rho_L a}\right)^{0.2}\right]$$

Equation 10

Correlation for film mass transfer coefficient is given as:

$$k_L = 0.0051\left(\frac{g\mu_L}{\rho_L}\right)^{1/3}\left(\frac{L_w}{a_w\mu_L}\right)^{2/3}\left(\frac{\mu_L}{D_L\rho_L}\right)^{-1/2}(ad_p)^{0.4}$$

Equation 11

$$k_G = K_5\frac{D_v a}{RT}\left(\frac{V_w}{a\mu_V}\right)^{0.7}\left(\frac{\mu_V}{D_v\rho_v}\right)^{1/3}(ad_p)^{-2.0}$$

Equation 12

Where, K_5 = 2.00 for packing sizes below 15 mm and 5.23 for above 15 mm,

L_w and V_w = liquid and gas mass flow rate per unit cross-sectional area, kg/m^2s,

a_w = effective interfacial area per unit volume of packing, m^2/ m^3

a = actual area per unit volume of packing, m^2/ m^3

d_p = packing size and is given as $d_p = 4*(\varepsilon/a)$; ε is void fraction, m^3/ m^3

and σ_c = critical surface tension based on packing material mN/m.

Based on the above correlations of film mass transfer coefficient and effective surface area, the film transfer unit heights are given as:

$H_G = \frac{G_m}{a_w k_G P}$ and $H_L = \frac{L_m}{a_w k_L C_t}$.

Equation 13

The results for the height of transfer unit for all packings calculated by Equation 9 are attached in appendix C. Table 9 summarizes the three best packings and shows the overall height of packing required for the corresponding cross-sectional area.

In order to make a direct comparison with benchmark scrubber, the above calculations were redone keeping the diameter of the column the same as that of scrubber. Since N_{OG} is essentially the ratio of the molar flow rates of gas and liquid phases per unit cross-sectional area, it remains constant. In theory, as the cross-sectional area increases the overall height of the tower should decrease. The results obtained are also in alignment of this expectation.

Table 9 Results of best packing material and the packing unit height for varying cross-sectional area of the tower. Calculated value of NTU is 4.87.

Tower diameter (m)	cross-sectional area (m^2)	Packing type	HTU (m)	Z = NTU x HTU (m)
1.1	1	Berl saddle – Ceramic - 13 mm	4.39	21.38
2.3 (half the scrubber diameter)	4.153	Berl saddle – Ceramic - 13 mm	3.24	15.78
3.25	8.31 (half the scrubber footprint)	Berl saddle – Ceramic - 13 mm	2.81	13.68
3.57	10	Berl saddle – Ceramic - 13 mm	2.70	13.12
4.6 (equivalent of scrubber diameter)	16.61	Berl saddle – Ceramic - 13 mm	2.44	11.9

It is important to note that there are significant constraints in the space requirement by the absorber or the scrubbers especially in the marine vehicles. Benchmark scrubber dimensions are 4.6 m diameter and 9 m height. Comparing it with an absorber tower of same diameter, the equivalent height of the packing unit is 11.98 m which is almost 3 m (30 %) higher than traditional scrubber. However, if we compare in terms of footprints, the space required for the absorber will be halved for the 4.6 m (50%) higher tower. Similarly, for a 15.8 m high packed tower, the foot print of the tower reduces to the quarter of the space occupied by the current scrubber unit. Thus, if the ships

can allow higher dimensions of the tower, significant decrease in the space allocation can be made possible.

Viscosity is an important factor affecting the mass transfer which can change the tower dimension requirement. For example, when the above tower design was done using properties at 25ºC, the tower design height with the same diameter as that of the scrubber gives a height of 15.36 m versus 11.9 meters, as designed by taking properties as 35ºC. Thus, it again highlights the importance of considering viscosity improver for a better and compact tower design.

With the use of alkali in scrubbing, a large space is required for the storage of the raw materials and the waste that is generated after SOx gas absorption. In case of using the recyclable solvent, raw material storage units will be significantly smaller as only a small amount is fresh IL-A might be required to be added. This tower design is readily suitable for large cargo ships especially those operating in ECA regions.

Chapter 6
CONCLUSIONS AND RECOMMENDATIONS

6.1 Conclusions:

Current SO_X gas abatement technology uses alkali solvents and generates alkali sulfite and alkali sulfates which are irreversible in nature. This project aimed to look at ionic liquids as recyclable solvents which will help curb down on the raw material requirement and on-site waste generation thus reducing the operational cost and meet the stringent IMO regulation that are to be implemented soon.

IL-A with additive-B was tested to absorb SO_2 gas and was proved to be partially recyclable. The additive was necessary to reduce the viscosity of the IL, especially after SO_2 absorption. Physical and chemical properties of the solvent-SO_2 systems with respect to temperatures were determined and a good understanding of the reaction mechanism was obtained using a combination of TGA and FTIR data. Equilibrium tests were successfully conducted to determine the capacity of IL-A for absorption which was determined to be 0.613 moles SO_2 to 1 mole of IL for 25ºC. Desorption of absorbed solvent was performed using nitrogen purging and about 0.42 moles of SO_2 per mole of IL-A was desorbed. This suggested that 0.2 moles were permanently absorbed by the IL-A, as it was not possible to remove them at least at the operating temperature pressure conditions. Recycling of the samples for 3 cycles indicated that after an initial loss in absorption capacity, the capacity remains almost steady for the subsequent two cycles. However, since only 3 cycles were performed it is advisable to comment after repeating for more number of cycles. Also, the current additive for improving the viscosity was observed to be more volatile than the IL-A through TGA

and FTIR results. It is necessary to take into account this additive loss when desorbing the solvent at higher temperatures.

Design calculations based on a 20 MW marine diesel engine exhaust was attempted for a packed tower. The results, in term of size, for similar performance were compared with traditional scrubber. A tower with ceramic berl saddle packing of 13 mm size gave the smallest tower design. The calculated height for the packed tower is 3 meters higher than the conventional scrubber with similar diameter. However, in term of the foot print, the packed tower has an advantage due to comparatively low requirements of waste storage and raw material requirements. New ships can be modified to accommodate the height of the tower and the packed tower design will off-set the initial cost of raw materials through it lower operational costs and more cargo space without switching to the high cost ULSFO fuel.

6.1 Recommendations:

This project looked at IL-A and additive-B as one of the primary ionic liquids for SO_2 abatement and it will act as a precursor in exploring other ionic liquids for similar applications. Taking insights from the current experimental data, additive-B proved to be a good viscosity improver but showed limitation of higher vapor pressure making it possible to explore other diluents having better stability and lower vapor pressure at higher temperature.

This project proceeded considering only N_2-SO_2 gas an ideal gas solution and did not consider the moisture and other gases such as CO_2 that are present in considerable amount. Tests in this direction of analyzing the effect of other gases particularly CO_2 can be considered and it will open the doors of custom blending of two ILs or multi-site ionic liquids for simultaneous gas scrubbing. These systems as is can be further improved by considering other design parameters and analyzing more packing materials to get an even better mass transfer resulting in more compact tower design.

Another interesting area would be to look at the desorption tower design. The method of desorption for the process design, by either N_2 purging or vacuum desorption will result into two different kinds of tower design i.e. either a desorber or Flash drum design. Furthermore, economic feasibility calculations will throw more light for better selection of desorption tower. A research into desorbed SO_2 storage is also an aspect unexplored in the project due to time constraint.

REFERENCES

Standard Operating Procedure for KSV SIGMA 701 FORCE. Retrieved from Force WebSite: Old documents: http://files.instrument.com.cn/17img/old/literature/C10549.pdf

A.V. Slack, H. F. (1972). Sulfur Oxide Removal from Waste Gases. *Journal of the Air Pollution Control Association*, 22 (3).

Ahmadreza. F. Ghobadi, V. T. (2011). Investigation on the Solubility of SO_2 and CO_2 in Imidazolium-Based Ionic Liquids Using NPT Monte Carlo Simulation. *The Journal of Physical Chemistry*, 115 (46), 13599-13607.

Air Pollution Control Technology Fact Sheet. Retrieved from www3.epa.gov: https://www3.epa.gov/ttncatc1/dir1/ffdg.pdf

Akyalcin, S. K. (2010). Flue gas desulfurization by citrate process and optimization of working parameters. *Chemical Engineering and Processing*, 49, 199-204.

Anirban Mondal, S. B. (2016). Understanding SO_2 Capture by Ionic Liquids. *The Journal of Physical Chemistry*, 120 (19), 4457-4466.

AP-42 VOL. I: 1.3: Fuel Oil Combustion. Retrieved from EPA Web site: https://www3.epa.gov/ttnchie1/ap42/ch01/final/c01s03.pdf

Aparicio, S., Alcalde, R., & Atilhan, M. (2010). Experimental and Computational Study on the Properties of Pure and Water Mixed 1-Ethyl-3-methylimidazolium l-(+)-Lactate Ionic Liquid. *The Journal of Physical Chemistry* , 114 (17), 5795-5809.

Barrosse-Antle, L. E., Silvester, D. S., Aldous, L., Hardacre, C., & Compton, R. G. (2008). Electroreduction of Sulfur Dioxide in Some Room-Temperature Ionic Liquids. *The Journal of Physical Chemistry* , 112 (9), 3398-3404.

Brookfield Digital Viscometer Model DV-E Operating Instructions. Retrieved from Cole parmer Web Site: Manual No. M/98-350-D0902: https://pim-resources.coleparmer.com/instruction-manual/98945-xx.pdf

Brown, J. D., & Straughan, B. P. (1972). A re-assignment of the fundamental frequencies of sodium sulphite. *J. Chem. Soc., Dalton Trans.*, 0, 1750-1751 .

Committee on Public Works. (1975). Chapter 6: The relatioship of sulfur oxide emissions to sulfur dioxide and sulfate air quality. In *Air quality and stationary source emission control* (233-271). Washington: U.S. Government Printing Office.

Elena Torralba-Calleja, J. S.-T. (2013). CO2 Capture in Ionic Liquids: A Review of Solubilities and Experimental Methods. *Journal of Chemistry*, Article ID 473584, 16 pages.

Fair, J. R., Steinmeyer, D. E., Penney, W. R., & Crocker, B. B. Gas Absorption and Gas-Liquid. In *Perry* Handbook of Chemical Engineering (p. 1999). The McGraw-Hill Companies, Inc.

Joan F. Brennecke, B. E. (2010). Ionic Liquids for CO2 Capture and Emission Reduction. *The Journal of Physical Chemistry Letters*, 1 (24), 3459-3464.

Kakusaburo Onda, H. T. (1968). Mass Transfer Coefficients Between Gas And Liquid Phases In Packed Columns . *Journal Of Chemical Engineering Of Japan* , 1(1), 56-62.

Kohl, A. L., & Nielsen, R. B. (1997). Ch. 7 Sulfur Dioxide Removal. In R. B. Kohl, *Gas Purification (Fifth Edition)* (466-669). Elsevier Inc.

Li, X., Zhang, L., Zheng, Y., & Zheng, C. (2015). Effect of SO2 on CO2 Absorption in Flue Gas by Ionic Liquid 1-Ethyl-3-methylimidazolium Acetate. *Industrial & Engineering Chemistry Research*, 54 (34), 8569-8578.

Matthew S. Shannon, J. E. (2011). Properties of Alkylimidazoles as Solvents for CO_2 Capture and Comparisons to Imidazolium-Based Ionic Liquids. *Industrial & Engineering Chemistry Research*, 50 (14), 8665-8677.

Matthew S. Shannon, J. E. (2012). Reactive and Reversible Ionic Liquids for CO_2 Capture and Acid Gas Removal. *Separation Science and Technology*, 47 (2).

National Research Council Canada. (2015). *Internal Report: SOx abatement using ionic liquids for marine applications (confidential).*

Ngo, H. L., LeCompte, K., Hargens, L., & McEwen, A. B. (2000). Thermal Properties of Imidazolium Ionic Liquids. *Thermochimica Acta*, 357-358(Issue) 97-102.

Onda, K., Takeuchi, H., & Okumoto, Y. (1968). Mass Transfer Coefficients between gas and liquid phases in Packed Columns. *Journal of Chemical Engineering of Japan*, 1(1) 56-62.

Paschoal, V. H., Faria, L. F., & Ribeiro, M. C. (2017). Vibrational Spectroscopy of Ionic Liquids. *Chemical reviews*, 117 (10), 7053 -7112.

Prevention of Air Pollution from Ships. Retrieved from International Maritime Organization: http://www.imo.org/en/OurWork/Environment/PollutionPrevention/AirPollution/Pages/Air-Pollution.aspx

R.Billet, & M.Schultes. (1999). Prediction of Mass Transfer Columns with Dumped and Arranged Packings: Updated Summary of the Calculation Method of Billet and Schultes. *Chemical Engineering Research and Design*, 77 (6), 498-504.

Randles, J. E. (1948). A cathode ray polarograph. Part II.—The current-voltage curves. *Trans. Faraday Soc.*, 44, 327-338.

S.Trasatti, & O.A.Petrii. (1992). Real surface area measurements in electrochemistry. *Journal of Electroanalytical Chemistry*, 327, 353-376.

Sargent and Lundy LLC. (2002, September). *Dry Flue Gas Desulfurization Technology Evaluation.* Retrieved from Graymont Web Site: http://www.graymont.com/sites/default/files/pdf/tech_paper/dry_flue_gas_desulfurization_technology_evaluation_0_1.pdf

Schmidt, K. A., & Mather, A. E. (2001). Solubility of sulphur dioxide in mixed polyethylene glycol dimethyl ethers. *The canadian Journal of Chemical Engineering*, 946–960.

Shiflett, M. B., Drew, D. W., Cantini, R. A., & Yokozeki, A. (2010). Carbon Dioxide Capture Using Ionic Liquid 1-Butyl-3-methylimidazolium Acetate. *Energy and Fuels*, 24 (10), 5781-5789.

Sinnott, R. K. (1993). *Coulson & Richardson Chemical Engineering design.* Oxford: Pergamon Press Ltd.

Sun, S., Niu, Y., Sun, Z., Xuc, Q., & Wei, X. (2015). Solubility properties and spectral characterization of sulfur dioxide in ethylene glycol derivatives. *RSC Advances*, 5, 8706-8712.

Sun, S., Niu, Y., Xu, Q., Suna, Z., & Wei, X. (2015). Highly efficient sulfur dioxide capture by glyme–lithium salt ionic liquids. *RSC Advances*, 5, 46564-46567.

Tang, M. J., Cox1, R. A., & Kalberer, M. (2014). Compilation and evaluation of gas phase diffusion coefficients of reactive trace gases in the atmosphere: volume 1. Inorganic compounds. *Atmos. Chem. Phys.*, 14, 9233-9247.

Wang, J. (2006). *Analytical Electrochemistry.* 3rd edition, Wiley VCH.

Wen Li, L. W. (2017). Using Ionic Liquid Mixtures To Improve the SO_2 Absorption Performance in Flue Gas. *Energy and Fuels*, 31 (2), 1771-1777.

Xu, Q., Xiao, J., Zhang, J., & Wei, X. (2016). Experimental solubility and absorption mechanism of dilute SO_2 in aqueous diethylene glycol dimethyl ether solution. *Korean Journal of Chemical Engineering*, 33 (12), 3493–3503.

Zeng, S., Zhang, X., Gao, H., He, H., Zhang, X., & Zhang, S. (2015). SO_2-Induced Variations in the Viscosity of Ionic Liquids Investigated by in Situ Fourier Transform Infrared Spectroscopy and Simulation Calculations. *Industrial & Engineering Chemistry Research*, 54 (43), 10854-10862.

Zhang, L., Zhang, Z., Sun, Y., Jiang, B., Li, X., Ge, X., & Wang, J. (2013). Ether-Functionalized Ionic Liquids with Low Viscosity for Efficient SO_2 Capture. *Industrial & Engineering Chemistry Research*, 52 (46), 16335-16340.

APPENDIX

Appendix A: TGA results for various samples:

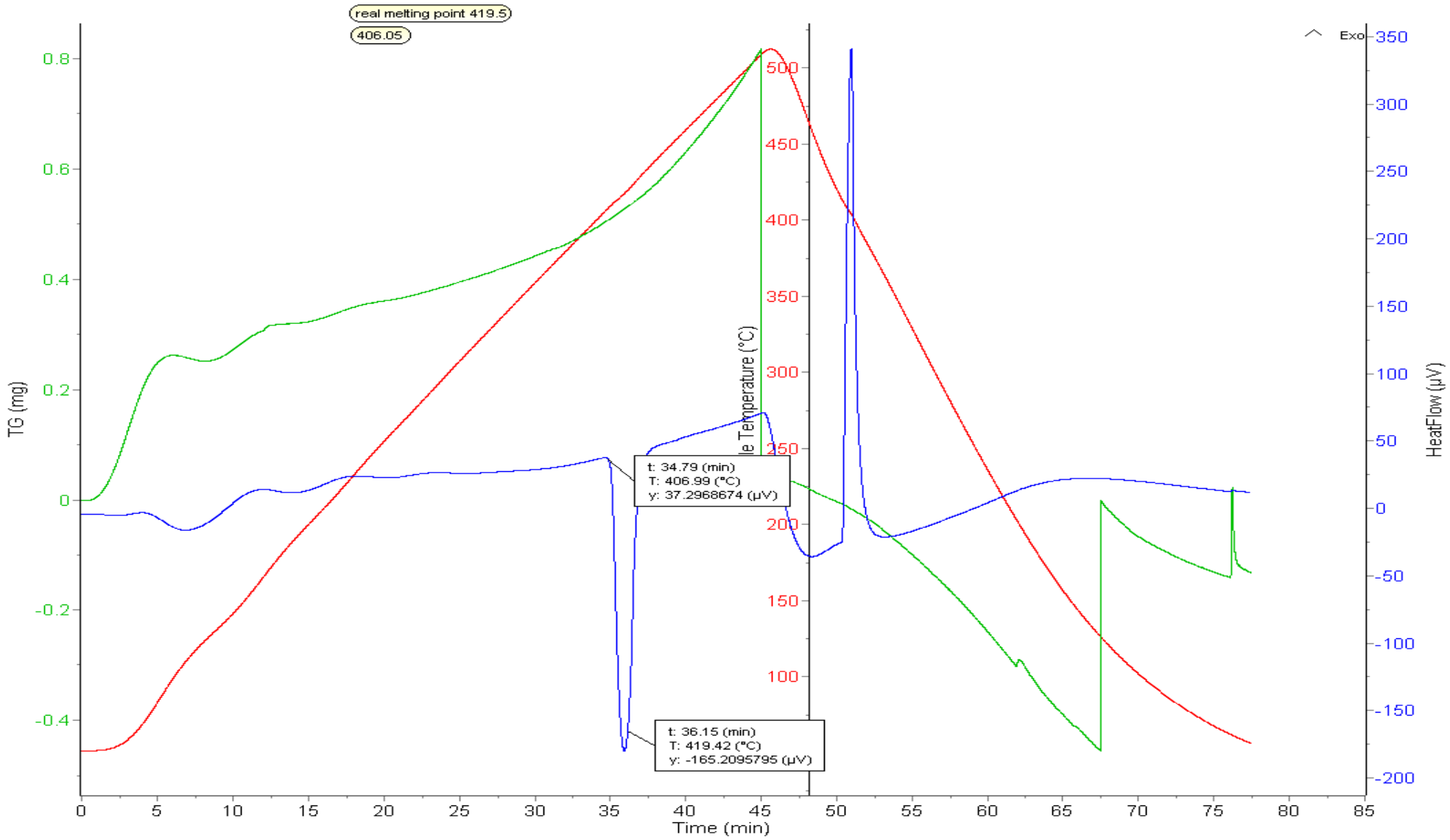

Figure 26 TGA of ultrapure Zn for equipment calibration

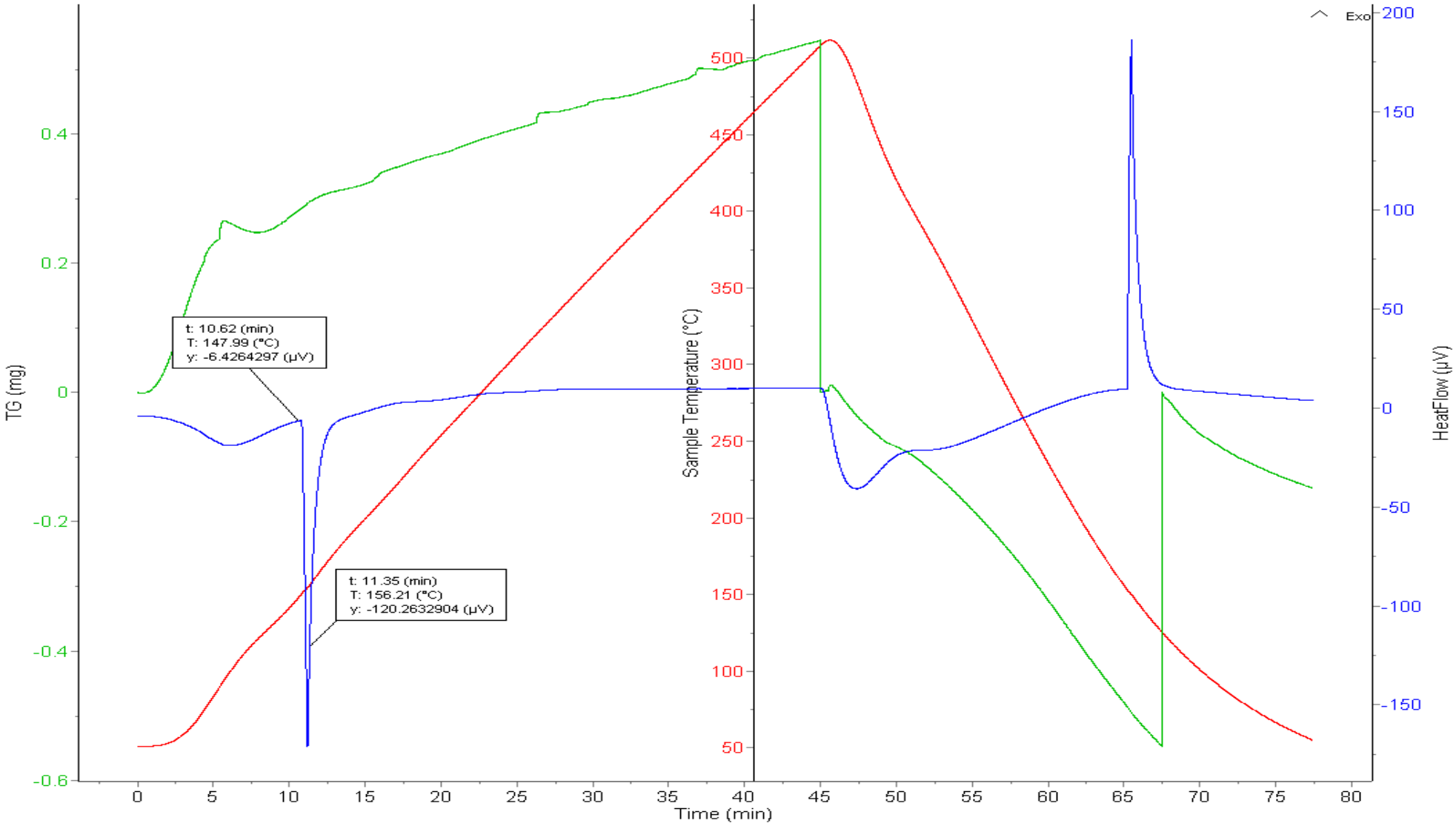

Figure 27 TGA of ultrapure In for equipment calibration

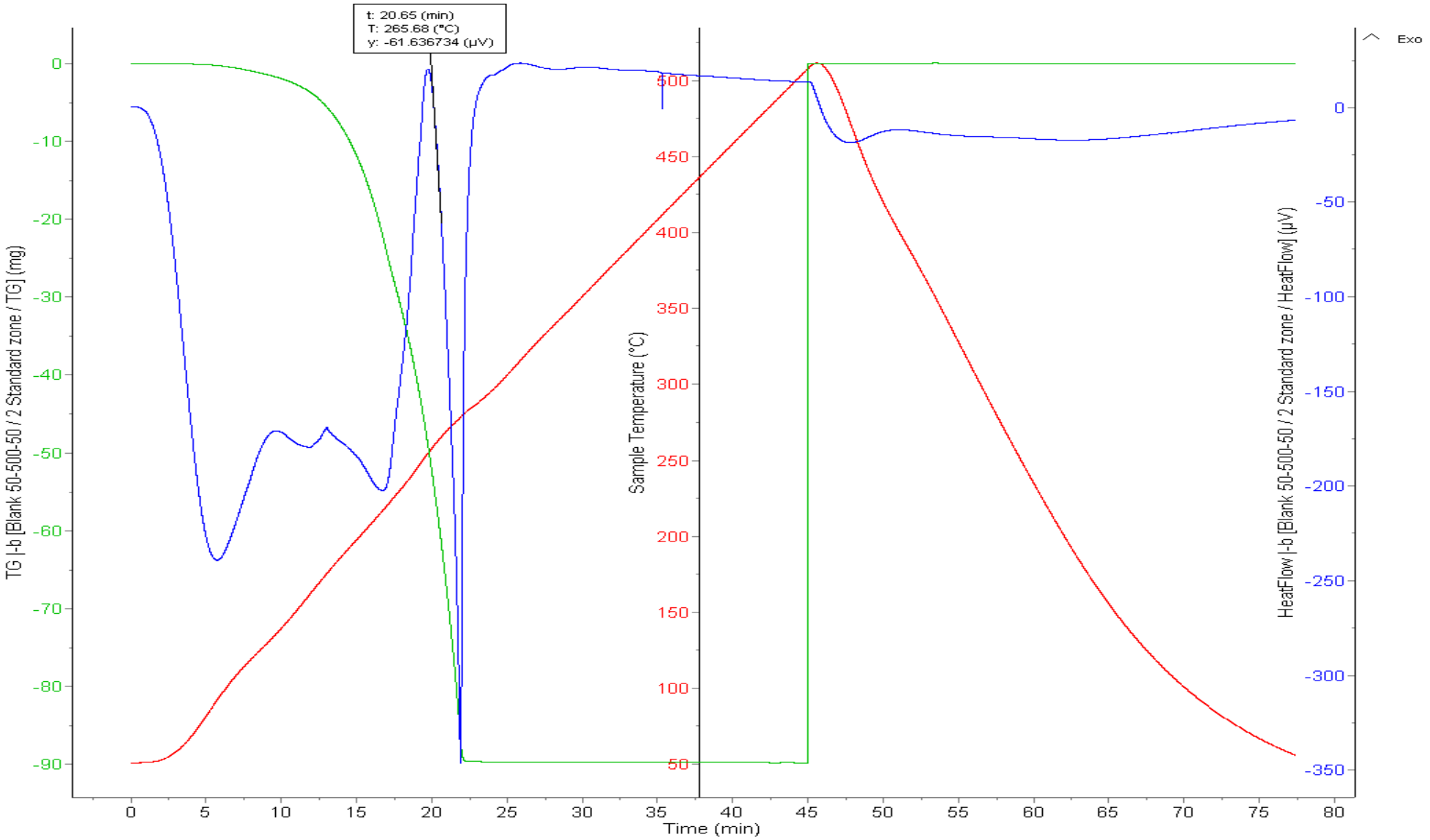

Figure 28 TGA of pure Additive for validation of calibration curve

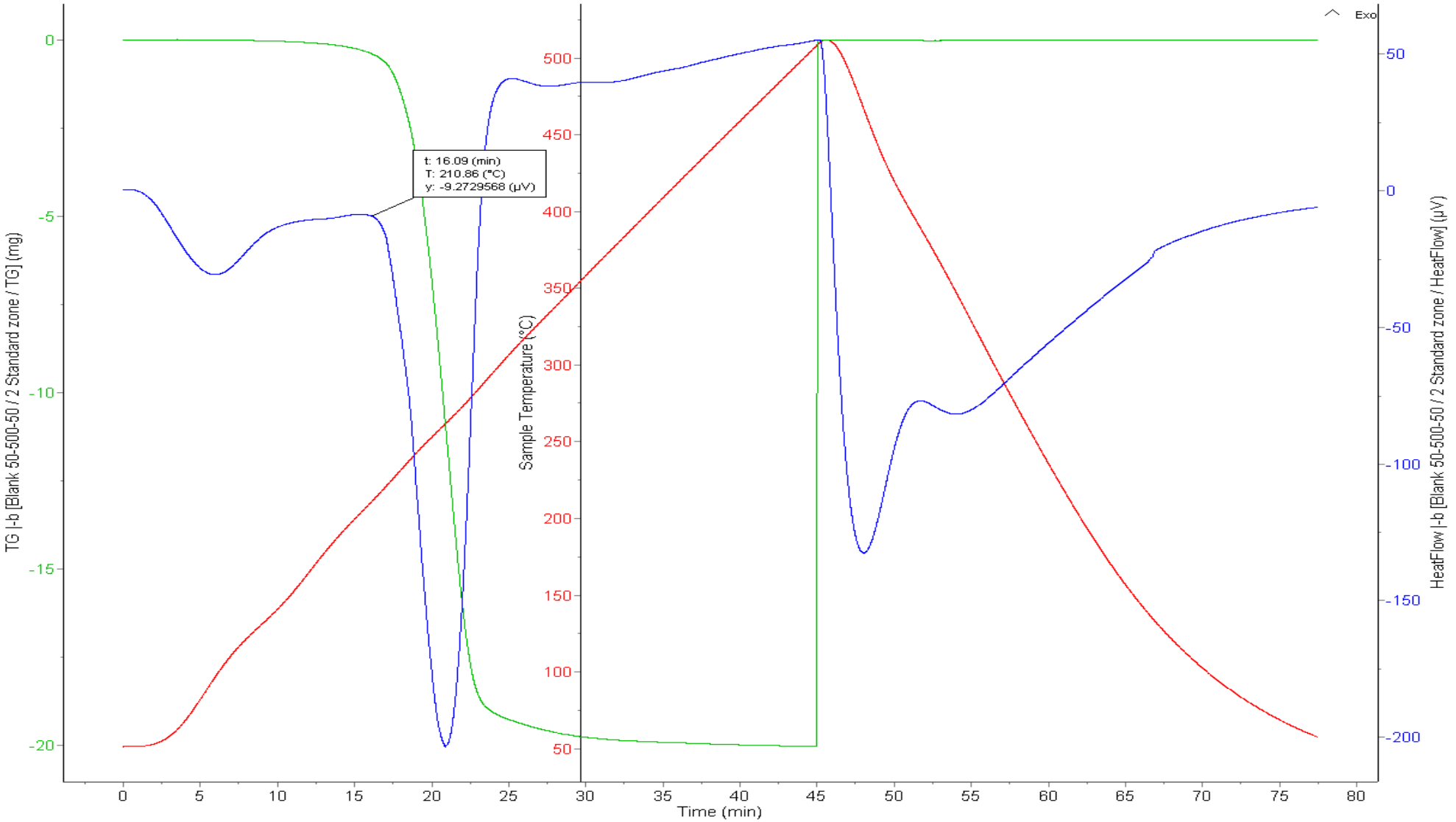

Figure 29 TGA analysis of IL-A to determine thermal stability

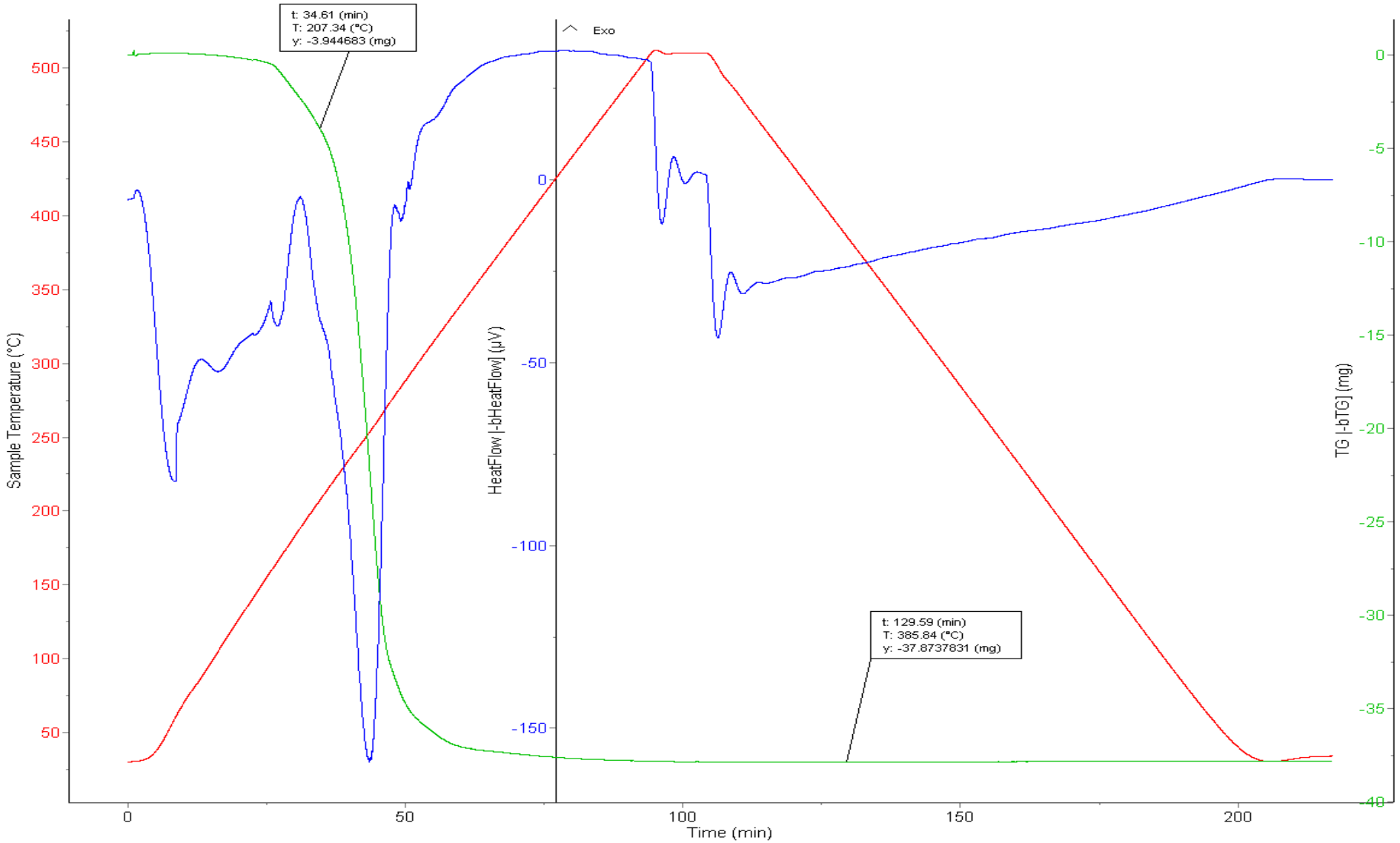

Figure 30 TGA analysis of cycled sample absorbed at 25 ºC and desorbed at 65 ºC

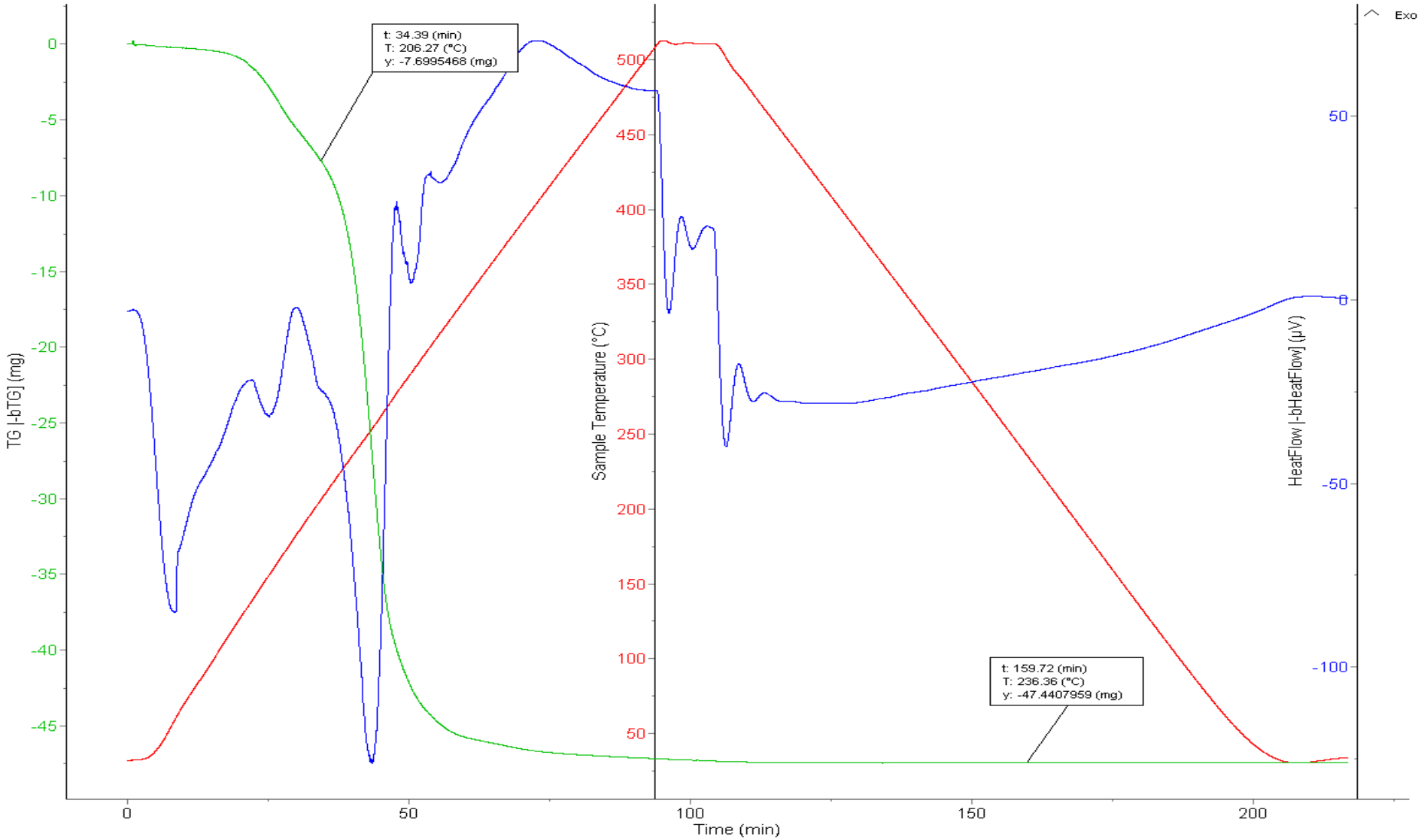

Figure 31 TGA analysis of cycled sample absorbed at 25 C and desorbed at 45 C

Appendix B: Experimental data for absorption equilibrium experiments:

For 25ºC absorption

Weight of setup	so2 weight gained	moles of so2	moles of IL	moles of additive	mole fraction of SO2
327.744					
330.557	0	0	0.101395	0.013698	0
330.605	0.048	0.000749	0.101395	0.013698	0.006467
330.688	0.131	0.002045	0.101395	0.013698	0.017455
330.728	0.171	0.002669	0.101395	0.013698	0.022664
330.916	0.359	0.005603	0.101395	0.013698	0.046424
331.037	0.48	0.007492	0.101395	0.013698	0.061115
331.246	0.689	0.010754	0.101395	0.013698	0.085452
331.378	0.821	0.012814	0.101395	0.013698	0.100183
331.624	1.067	0.016654	0.101395	0.013698	0.126407
331.747	1.19	0.018573	0.101395	0.013698	0.138953
332.767	2.21	0.034494	0.101395	0.013698	0.230592
332.77	2.213	0.03454	0.101395	0.013698	0.230833
332.881	2.324	0.036273	0.101395	0.013698	0.239637
333.133	2.576	0.040206	0.101395	0.013698	0.258894
333.233	2.676	0.041767	0.101395	0.013698	0.266268
333.482	2.925	0.045653	0.101395	0.013698	0.284008
333.567	3.01	0.04698	0.101395	0.013698	0.289868
334.283	3.726	0.058155	0.101395	0.013698	0.335675
334.322	3.765	0.058764	0.101395	0.013698	0.338001
334.399	3.842	0.059966	0.101395	0.013698	0.342546
334.415	3.858	0.060215	0.101395	0.013698	0.343482
334.452	3.895	0.060793	0.101395	0.013698	0.345638
334.463	3.906	0.060965	0.101395	0.013698	0.346276
334.472	3.915	0.061105	0.101395	0.013698	0.346797
334.48	3.923	0.06123	0.101395	0.013698	0.34726
334.482	3.925	0.061261	0.101395	0.013698	0.347375

For 35ºC absorption

Weight	so2 weight gained	moles of so2	moles of IL	moles of Diluent	mole fraction of SO2
325.991	0	0	0.10241	0.016279	0
326.076	0.085	0.001327	0.10241	0.016279	0.011054147
326.136	0.145	0.002263	0.10241	0.016279	0.018711073
326.363	0.372	0.005806	0.10241	0.016279	0.046637452
326.436	0.445	0.006946	0.10241	0.016279	0.055283472
326.587	0.596	0.009302	0.10241	0.016279	0.072679185
326.817	0.826	0.012892	0.10241	0.016279	0.097978486
327.84	1.849	0.028859	0.10241	0.016279	0.195590547
327.9	1.909	0.029796	0.10241	0.016279	0.200663859
328.04	2.049	0.031981	0.10241	0.016279	0.212256335
328.093	2.102	0.032808	0.10241	0.016279	0.216557654
328.221	2.23	0.034806	0.10241	0.016279	0.226754554
328.27	2.279	0.03557	0.10241	0.016279	0.230588148
328.384	2.393	0.03735	0.10241	0.016279	0.239361704
328.427	2.436	0.038021	0.10241	0.016279	0.242619281
328.513	2.522	0.039363	0.10241	0.016279	0.249051439
328.56	2.569	0.040097	0.10241	0.016279	0.252520732
328.94	2.949	0.046028	0.10241	0.016279	0.279435425
328.986	2.995	0.046746	0.10241	0.016279	0.282562574
329.105	3.114	0.048603	0.10241	0.016279	0.290527837
329.139	3.148	0.049134	0.10241	0.016279	0.292771244
329.148	3.157	0.049274	0.10241	0.016279	0.293362714
329.154	3.163	0.049368	0.10241	0.016279	0.293756478

For 65ºC absorption

Weight of setup	so2 dissolved	moles of so2	moles of IL	moles of Diluent	mole fraction of SO2
285.57					
285.51	0	0	0.10445	0.016604	0
285.529	0.019	0.000297	0.10445	0.016604	0.00244376
285.555	0.045	0.000702	0.10445	0.016604	0.005768562
285.592	0.082	0.00128	0.10445	0.016604	0.01046198
285.642	0.132	0.00206	0.10445	0.016604	0.016734483
285.679	0.169	0.002638	0.10445	0.016604	0.021325178
285.763	0.253	0.003949	0.10445	0.016604	0.031589839
286.017	0.507	0.007913	0.10445	0.016604	0.06135857
286.27	0.76	0.011862	0.10445	0.016604	0.089244778
286.332	0.822	0.01283	0.10445	0.016604	0.095827601
286.378	0.868	0.013548	0.10445	0.016604	0.100650467
286.417	0.907	0.014156	0.10445	0.016604	0.104699297
286.453	0.943	0.014718	0.10445	0.016604	0.108404456
286.492	0.982	0.015327	0.10445	0.016604	0.112383926
286.545	1.035	0.016154	0.10445	0.016604	0.117735327
286.605	1.095	0.017091	0.10445	0.016604	0.123716171
286.642	1.132	0.017668	0.10445	0.016604	0.127364106
286.696	1.186	0.018511	0.10445	0.016604	0.132633939
286.742	1.232	0.019229	0.10445	0.016604	0.137073109
286.795	1.285	0.020056	0.10445	0.016604	0.142131798
286.814	1.304	0.020353	0.10445	0.016604	0.143930879
286.851	1.341	0.02093	0.10445	0.016604	0.147412784
286.915	1.405	0.021929	0.10445	0.016604	0.153369137
286.951	1.441	0.022491	0.10445	0.016604	0.156683156
287.015	1.505	0.02349	0.10445	0.016604	0.162511126
287.052	1.542	0.024067	0.10445	0.016604	0.165843822
287.108	1.598	0.024941	0.10445	0.016604	0.170837752
287.124	1.614	0.025191	0.10445	0.016604	0.172253625
287.294	1.784	0.027845	0.10445	0.016604	0.187003971

287.331	1.821	0.028422	0.10445	0.016604	0.190144949
287.353	1.843	0.028765	0.10445	0.016604	0.192001079
287.433	1.923	0.030014	0.10445	0.016604	0.198679512
287.462	1.952	0.030467	0.10445	0.016604	0.201073262
287.482	1.972	0.030779	0.10445	0.016604	0.202715808

For 25ºC desorption

Weight of setup	so2 weight lost	moles of so2 lost	moles of IL	moles of Diluent	mole fraction of SO2 lost
334.482	0	0	0.101395	0.013698	0
334.386	0.096	0.001498	0.101395	0.013698	0.012851369
333.892	0.59	0.009209	0.101395	0.013698	0.074083178
333.862	0.62	0.009677	0.101395	0.013698	0.077557963
333.791	0.691	0.010785	0.101395	0.013698	0.085678634
333.765	0.717	0.011191	0.101395	0.013698	0.08861675
333.703	0.779	0.012159	0.101395	0.013698	0.095547403
333.686	0.796	0.012424	0.101395	0.013698	0.097429368
333.636	0.846	0.013204	0.101395	0.013698	0.102919442
333.618	0.864	0.013485	0.101395	0.013698	0.104879555
333.586	0.896	0.013985	0.101395	0.013698	0.108343132
333.566	0.916	0.014297	0.101395	0.013698	0.110494289
333.432	1.05	0.016388	0.101395	0.013698	0.124643561
333.426	1.056	0.016482	0.101395	0.013698	0.125266589
333.4	1.082	0.016888	0.101395	0.013698	0.12795616
333.386	1.096	0.017106	0.101395	0.013698	0.129397551
333.348	1.134	0.017699	0.101395	0.013698	0.133285987
333.352	1.13	0.017637	0.101395	0.013698	0.132878314
333.33	1.152	0.01798	0.101395	0.013698	0.135115779
333.323	1.159	0.01809	0.101395	0.013698	0.135825281
333.263	1.219	0.019026	0.101395	0.013698	0.141859303
333.19	1.292	0.020165	0.101395	0.013698	0.149088027
333.189	1.293	0.020181	0.101395	0.013698	0.149186205
333.15	1.332	0.02079	0.101395	0.013698	0.15299756
333.142	1.34	0.020915	0.101395	0.013698	0.153775159
333.138	1.344	0.020977	0.101395	0.013698	0.154163424

For 35ºC desorption

Weight	**so2 weight lost**	**moles of so2 lost**	**moles of IL**	**moles of Diluent**	**mole fraction of SO2 lost**
329.884	0	0	0.10241	0.016279	0
329.769	0.115	0.001794912	0.10241	0.016279	0.014897
329.518	0.366	0.005712502	0.10241	0.016279	0.04592
329.495	0.389	0.006071484	0.10241	0.016279	0.048665
329.145	0.739	0.011534259	0.10241	0.016279	0.088573
329.122	0.762	0.011893242	0.10241	0.016279	0.091078
329.082	0.802	0.012517559	0.10241	0.016279	0.095403
329.059	0.825	0.012876541	0.10241	0.016279	0.097871
329.019	0.865	0.013500858	0.10241	0.016279	0.102132
328.994	0.89	0.013891057	0.10241	0.016279	0.104775
328.962	0.922	0.01439051	0.10241	0.016279	0.108134
328.956	0.928	0.014484158	0.10241	0.016279	0.108762
328.923	0.961	0.01499922	0.10241	0.016279	0.112195
328.906	0.978	0.015264554	0.10241	0.016279	0.113954
328.808	**1.076**	**0.016794131**	0.10241	0.016279	0.123957
328.808	1.076	0.016794131	0.10241	0.016279	0.123957

For 45ºC absorption

Weight	so2 weight lost	moles of so2 lost	moles of IL	moles of Diluent	mole fraction of SO2 lost
333.138	1.344	0.020977056	0.101395	0.013698	0.154163
332.966	1.516	0.02366162	0.101395	0.013698	0.170528
332.947	1.535	0.023958171	0.101395	0.013698	0.172297
332.867	1.615	0.025206805	0.101395	0.013698	0.179664
332.847	1.635	0.025518964	0.101395	0.013698	0.181485
332.571	1.911	0.029826752	0.101395	0.013698	0.205815
332.557	1.925	0.030045263	0.101395	0.013698	0.207011
332.531	1.951	0.030451069	0.101395	0.013698	0.209222
332.517	1.965	0.03066958	0.101395	0.013698	0.210407
332.478	2.004	0.031278289	0.101395	0.013698	0.213691
332.464	2.018	0.0314968	0.101395	0.013698	0.214863
332.439	2.043	0.031886999	0.101395	0.013698	0.216948
332.424	2.058	0.032121118	0.101395	0.013698	0.218193
332.312	2.17	0.033869206	0.101395	0.013698	0.227367
332.306	2.176	0.033962853	0.101395	0.013698	0.227853
332.288	2.194	0.034243796	0.101395	0.013698	0.229306
332.283	2.199	0.034321835	0.101395	0.013698	0.229708
332.267	2.215	0.034571562	0.101395	0.013698	0.230993
332.262	2.22	0.034649602	0.101395	0.013698	0.231394
332.246	2.236	0.034899329	0.101395	0.013698	0.232674
332.241	2.241	0.034977369	0.101395	0.013698	0.233073
332.228	2.254	0.035180272	0.101395	0.013698	0.234108
332.226	2.256	0.035211487	0.101395	0.013698	0.234267
332.154	2.328	0.036335258	0.101395	0.013698	0.23995
332.15	2.332	0.03639769	0.101395	0.013698	0.240263
332.138	2.344	0.036584985	0.101395	0.013698	0.241201
332.135	2.347	0.036631809	0.101395	0.013698	0.241436
332.125	2.357	0.036787888	0.101395	0.013698	0.242215

Appendix C: MATLAB code for mathematical absorption design:

```
function result = loading

%for 85% IL absorption


Dl  = 1207.7; %density of solvent phase kg/m3

Dv  = 1.184;  %density of gas phase kg/m3

g   = 9.81;   % gravitational force constant m/s

A = 1 %area m2

V = 2513.598; %kmol/hr

Vm = 2513.598/(A*3600); %kmol/m2s

Ml = 189.377; %Mwt of solvent stream

Mv = 29.023; %Mwt of gas stream


Vms = Vm * Mv; %kg/m2s

y1 = 0.00005; %Mol fraction of SO2 in top of the tower

y2 = 0.0018;  %Mol frction of SO2 at the bottom of the tower

x1 = 0.0627;  %Mol fraction of So2 in inlet solvent stream

x2 = 0.3;     %Mol fraction of So2 in outlet solvent stream

Vl  = 0.0818; %Viscosity of the solvent stream kg/m-s
```

```
Vv  = 0.000019/Dv; %Viscosity of the gas stream kg/m-s

STl = 0.034595; %surface tension of solvent stream kg/s2

m = 0.0052; %.....slope of the equilibrium line

R = 0.08206; % gas constant atm m3/kmolK

T = 308.15; % absorption temperature K

Dffl =  0.00000000128;% liquid phase diffusivilty coefficient

Dffv =  0.0000134415;% gas phase diffusivilty coefficient

datasave=[];
i = 1;
fprintf('  aw       kG       kL       HG       HL       Hog       Nog       Z \n')

load('onda.mat')

for n = i:69
   i= i+1;

a = unnamed(i,2);
K5 = unnamed(i,5);
sC = unnamed(i,4);
E = unnamed(i,3);




% minimun solvent calculations
Lmin = Vm*((y1-y2)/(x1-x2));

Lm = (Lmin * 2)%kmol/m2s
```

```
Lms = Lm * Ml; %kg/m2s



% NTU calculations

Q = m*(Vm/Lm);
X = ((1-Q)*(y2/y1))+ Q;

Nog = (1/(1-Q))*log(X);



% HTU calculations

 dp = 4*(E/a);   % Billet and Schultz paper

%calulating effective area per packing aw

aw = a*(1-exp(-1.45*(((sC/1000)/STl)^0.75)*((Lms/a*Vl)^0.1)*((Lms*Lms*a/Dl*Dl*g)^(-
0.05))*((Lms*Lms/Dl*STl*a)^(0.2))));

%calculating kG; gas film mass transfer coefficent

kG = (K5*a*Dffv/(R*T))*((Vms/(a*Vv))^(0.7))*((Vv/(Dv*Dffv))^0.33)*(a*dp)^-2;

%calculating kL; gas film mass transfer coefficent

kL = 0.0051*(((Vl*g)/Dl)^0.33)*((Lms/(aw*Vl))^(0.66))*((Vl/(Dl*Dffl))^-0.5)*(a*dp)^0.4;


HG = Vm/(kG*aw);
```

```
HL = Lm/(kL*aw*(Dl/189.377));

Hog = HG + (m*Vm*HL/Lm);



% overall Height of packing unit

Z = Nog * Hog;



format SHORT

datasave=[datasave;aw kG kL HG HL Hog Nog Z];
end

disp(datasave)


filename = 'Final_abs85.xlsx';
xlswrite(filename,datasave)
end
```

Sample result for overall height of packed tower (Z) (of unit cross sectional area) for various types of packing materials:

Dumped Packings	**MOC**	**Size (mm)**	**N**	**aw**	**Hg**	**Hl**	**Hog**	**Nog**	**Z (m)**
Raschig Super-Ring	Metal	0.3	180000	100.953	0.913	12.138	5.192	4.887	25.373
Raschig Super-Ring	Metal	0.5	145000	79.366	1.284	13.092	5.899	4.887	28.827
Raschig Super-Ring	Metal	1	32000	49.870	2.359	15.301	7.754	4.887	37.890
Raschig Super-Ring	Metal	2	9500	29.805	4.625	18.190	11.039	4.887	53.941
Raschig Super-Ring	Metal	3	4300	24.230	6.003	19.541	12.892	4.887	62.999
Raschig Super-Ring	Plastic	2	9000	17.889	7.267	21.862	14.975	4.887	73.175
Ralu Flow	Plastic	1	33000	30.193	3.552	18.452	10.058	4.887	49.150
Ralu Flow	Plastic	2	4600	17.889	7.042	22.000	14.798	4.887	72.312
Pall ring	Metal	50	6242	34.590	1.361	17.537	7.544	4.887	36.864
Pall ring	Metal	35	19517	43.203	1.052	16.165	6.752	4.887	32.993
Pall ring	Metal	25	53900	70.627	0.546	13.740	5.390	4.887	26.341
Pall ring	Plastic	50	6765	19.970	2.210	21.430	9.766	4.887	47.722
Pall ring	Plastic	35	17000	27.539	1.421	19.321	8.232	4.887	40.229
Pall ring	Plastic	25	52300	41.751	0.797	16.915	6.761	4.887	33.037
Ralu ring	Metal	50	6300	32.162	1.571	17.798	7.846	4.887	38.341
Ralu ring	Metal	38	14500	41.784	1.099	16.350	6.863	4.887	33.537
Ralu ring	Metal	25	51000	67.833	0.583	13.895	5.482	4.887	26.786

Ralu ring	Plastic	50	5770	16.993	3.113	22.037	10.883	4.887	53.179
Ralu ring	Plastic	38	13500	27.330	1.512	19.170	8.270	4.887	40.413
Ralu ring	Plastic	25	36000	34.989	1.124	17.550	7.311	4.887	35.727
NOR PAC ring	Plastic	50	7330	15.429	3.272	23.115	11.421	4.887	55.811
NOR PAC ring	Plastic	35	17450	25.770	1.680	19.440	8.534	4.887	41.701
NOR PAC ring	Plastic	25	50000	37.302	1.064	17.078	7.085	4.887	34.621
NOR PAC ring	Plastic	25	48920	36.511	1.019	17.448	7.170	4.887	35.038
Hi• ow-ring	Metal	50	5000	28.122	1.876	18.614	8.438	4.887	41.234
Hi• ow-ring	Metal	25	40790	63.863	0.632	14.172	5.629	4.887	27.504
Hi• ow-ring	Metal	50	6815	36.031	1.222	17.488	7.387	4.887	36.099
Hi• ow-ring	Plastic	50 hydr.	6890	21.343	2.056	20.896	9.423	4.887	46.046
Hi• ow-ring	Plastic	50 S	6050	14.538	3.495	23.637	11.828	4.887	57.800
Hi• ow-ring	Plastic	25	46100	35.856	1.038	17.571	7.233	4.887	35.346
Hi• ow-ring	Ceramic	50	5120	23.960	1.522	21.197	8.995	4.887	43.957
Hi• ow-ring	Ceramic	38	13241	30.145	1.075	19.812	8.059	4.887	39.384
Hi• ow-ring	Ceramic	20	121314	80.306	0.282	14.421	5.366	4.887	26.220
Glitsch ring	Metal	30 PMK	29200	56.540	0.760	14.692	5.939	4.887	29.024
Glitsch ring	Metal	30 P	31100	51.169	0.836	15.300	6.230	4.887	30.443
Glitsch CMR ring	Metal	1.5"	60744	54.715	0.791	14.863	6.031	4.887	29.470

Glitsch CMR ring	Metal	1.5" T	63547	58.988	0.715	14.499	5.827	4.887	28.473
Glitsch CMR ring	Metal	1.0"	158467	73.591	0.537	13.454	5.280	4.887	25.802
Glitsch CMR ring	Metal	0.5"	560811	114.666	0.762	11.663	4.874	4.887	23.816
TOP Pak ring	Alu	50	6871	32.322	1.501	17.909	7.815	4.887	38.188
Raschig ring	Ceramic	50	5990	25.438	1.483	20.558	8.731	4.887	42.667
Raschig ring	Ceramic	25	47700	52.397	0.393	17.414	6.532	4.887	31.921
VSP ring	Metal	50	7841	32.035	1.596	17.786	7.866	4.887	38.439
VSP ring	Metal	25	33434	62.782	0.664	14.178	5.662	4.887	27.670
Envi Pac ring	Plastic	80	2000	10.488	5.468	26.268	14.729	4.887	71.975
Envi Pac ring	Plastic	60	6800	17.590	2.846	21.978	10.594	4.887	51.771
Envi Pac ring	Plastic	32	53000	25.220	1.698	19.650	8.626	4.887	42.152
Bialecki ring	Metal	50	6278	37.281	1.275	16.989	7.265	4.887	35.501
Bialecki ring	Metal	35	18200	48.248	0.917	15.557	6.401	4.887	31.281
Bialecki ring	Metal	25	48533	66.191	0.596	14.035	5.544	4.887	27.094
Tellerette	Plastic	25	37037	34.989	1.100	17.626	7.314	4.887	35.740
Hackette	Plastic	45	12000	25.334	1.659	19.688	8.601	4.887	42.028
Ra• ux ring	Plastic	15	193522	57.947	0.531	15.084	5.849	4.887	28.581
Berl saddle	Ceramic	25	80080	72.660	0.258	15.582	5.751	4.887	28.105
Berl saddle	**Ceramic**	**13**	**691505**	157.128	0.087	12.206	4.391	4.887	21.455
DIN-PAK	Plastic	70	9763	19.895	2.314	21.282	9.817	4.887	47.974

DIN-PAK	Plastic	47	28168	23.760	1.783	20.165	8.892	4.887	43.453
Pall ring	Ceramic	50	7502	42.435	0.633	17.951	6.962	4.887	34.022
Bialecki ring	Metal	35	20736	55.268	0.735	14.992	6.020	4.887	29.420
Ralu pak	Metal	YC-250		79.366	0.461	13.256	5.135	4.887	25.092
Mellapak	Metal	250Y		79.366	0.486	13.119	5.111	4.887	24.975
Gempack	Metal	A2T-304		63.568	0.656	14.106	5.629	4.887	27.508
Impulse packing	Metal	250		79.366	0.491	13.092	5.106	4.887	24.953
Impulse packing	Ceramic	100		24.434	1.593	20.761	8.912	4.887	43.551
Montz packing	Metal	B1-200		62.913	0.667	14.144	5.654	4.887	27.630
Montz packing	Metal	B2-300		95.954	0.350	12.508	4.759	4.887	23.258
Montz packing	Plastic	C1-200		36.916	1.080	17.132	7.120	4.887	34.794
Montz packing	Plastic	C2-200		36.916	0.961	17.536	7.144	4.887	34.909
Euroform	Plastic	PN-110		19.763	2.324	21.349	9.851	4.887	48.136